CRYSTAL-CHEMICAL AND THERMAL CONTROLS ON TRACE-ELEMENT PARTITIONING BETWEEN COEXISTING GARNET AND BIOTITE IN METAMORPHIC ROCKS FROM WESTERN LABRADOR

PANSEOK YANG[§], TOBY RIVERS AND SIMON JACKSON[†]

Department of Earth Sciences, Memorial University of Newfoundland, St. John's, Newfoundland A1B 3X5

ABSTRACT

Trace-element concentrations of coexisting garnet and biotite in thirteen metamorphic rocks from western Labrador, ranging from lower-greenschist to upper-amphibolite facies, were determined by laser-ablation microprobe – inductively coupled plasma – mass spectrometry (LAM–ICP–MS). Systematic trace-element distributions across wide compositional and thermal ranges suggest that equilibrium was approached during metamorphic crystallization. Zn depletion in garnet and biotite from staurolite-bearing assemblages demonstrates the control of mineral assemblage on the concentrations of trace elements. Mean molar distribution coefficients [(D_i^*(garnet/biotite)] from greenschist-facies assemblages have the following values: Sc 5.03 ± 1.27 (1σ), Eu 1.99 ± 1.69, Cr 0.83 ± 0.53, V 0.39 ± 0.13, Co 0.27 ± 0.07 and Zn 0.12 ± 0.02. For upper-amphibolite-facies assemblages, the D_i^* values are: Sc 8.98 ± 7.08, Eu 64.77 ± 41.66, Cr 0.88 ± 0.56, V 0.17 ± 0.06, Co 0.46 ± 0.08 and Zn 0.15 ± 0.03. Other trace elements have concentrations near or below detection limits in either garnet or biotite. The partition of Sc and Ti between garnet and biotite is controlled by the contents of ^{IV}Al in biotite and Ca in garnet, respectively, indicating that crystal chemistry exerts an influence on trace-element partitioning. In contrast, the partition of Co and Zn shows a thermal dependence and is less sensitive to compositional changes in the host minerals. Distribution coefficients for Zr, Sm, Eu and Gd between garnet and biotite vary systematically with both the Mg/(Mg + Fe) values of garnet and biotite as well as with metamorphic temperature; it was not possible to isolate these two competing factors. The partition of elements between coexisting garnet and biotite is strongly controlled by crystal structure, so that the distribution of elements occupying each cation site in the garnet structure is characterized by a parabola-shaped peak in a diagram where distribution coefficients are plotted against ionic radius. Our study indicates that some instances of irregular partitioning of trace elements between garnet and biotite, found in previous work utilizing bulk analyses of mineral separates, may have been due to inclusions, impurities, and zoning involving trace elements.

Keywords: trace elements, garnet, biotite, laser-ablation microprobe, ICP–MS, distribution coefficients, crystal chemistry, thermal dependence, crystal structure, Labrador.

SOMMAIRE

La concentration d'éléments traces dans le grenat et la biotite coexistants dans treize échantillons de roches métamorphiques provenant de l'ouest du Labrador, dont le degré de métamorphisme va du faciès schistes verts inférieur au faciès amphibolite supérieur, a été déterminé par ablation au laser et analyse de plasma à couplage inductif, avec spectrométrie de masse (LAM–ICP–MS). Les distributions systématiques de ces éléments traces, malgré les divergences importantes en composition globale et degré de réchauffement métamorphique, font penser qu'il y a eu une approche à l'équilibre. L'appauvrissement du grenat et de la biotite en Zn dans les assemblages à staurolite démontre l'importance que peut exercer les minéraux sur les concentrations d'éléments traces. Exprimés sur une base molaire, voici les coefficients moyens de distribution [(D_i^*(grenat/biotite)] dérivés d'assemblages du faciès schistes verts: Sc 5.03 ± 1.27 (1σ), Eu 1.99 ± 1.69, Cr 0.83 ± 0.53, V 0.39 ± 0.13, Co 0.27 ± 0.07 et Zn 0.12 ± 0.02. Dans le cas des assemblages du faciès amphibolite supérieur, les valeurs de D_i^* sont: Sc 8.98 ± 7.08, Eu 64.77 ± 41.66, Cr 0.88 ± 0.56, V 0.17 ± 0.06, Co 0.46 ± 0.08 et Zn 0.15 ± 0.03. Les concentrations d'autres éléments traces sont proches ou bien en dessous du seuil de détection, soit pour le grenat, soit pour la biotite. La répartition du Sc et du Ti entre grenat et biotite est régie par la teneur en ^{IV}Al de la biotite et en Ca du grenat, respectivement, indication du rôle que peut exercer la cristallochimie sur la répartition des éléments traces. En revanche, la répartition du Co et du Zn démontre une dépendance de la température, et serait moins sensible aux changements de composition des minéraux métamorphiques hôtes. Les coefficients de partage pour le Zr, Sm, Eu et Gd entre grenat et biotite varient systématiquement selon la valeur du rapport Mg/(Mg + Fe) du grenat et de la biotite, de même que la température de réchauffement maximale; il ne nous a pas été possible de distinguer les effets de ces deux variables. La répartition d'éléments entre grenat et biotite coexistants dépendrait fortement de la structure cristalline; dans chaque

[†] *Present address*: School of Earth Sciences, Macquarie University, Sydney, N.S.W. 2109, Australia

[§] *E-mail address*: pyang@plato.ucs.mun.ca

site de la structure du grenat, par exemple, la distribution des éléments définit un maximum d'aspect parabolique dans un diagramme où l'on reporte les coefficients de distribution en fonction du rayon ionique. D'après nos résultats, une répartition irrégulière d'éléments entre grenat et biotite, établis dans certains cas lors d'études antérieures fondées sur l'analyse de concentrés de minéraux, pourrait bien témoigner de la présence d'inclusions, d'impuretés, et de zonation impliquant les éléments traces.

INTRODUCTION

The distribution of trace elements has great potential in the study of metamorphic assemblages and the P–T–X conditions of metamorphism because they are usually more sensitive to metamorphic reactions and the local chemical environments than major elements (Hickmott & Shimizu 1990, Hickmott & Spear 1992, Lanzirotti 1995, Schwandt *et al.* 1996). For example, trace-element zoning is known to be a useful monitor of metamorphic reaction-history where trace-element-enriched refractory minerals are involved in the reactions (Hickmott & Spear 1992). In addition, in a classic study, Kretz (1959) showed that equilibrium trace-element partitioning among coexisting metamorphic minerals has the potential to reflect metamorphic grade. On the basis of his and other data, Kretz (1961) developed the thermodynamic theory for the equilibrium distribution of trace elements between coexisting metamorphic minerals, and in so doing demonstrated quantitatively the potential of trace-element thermometry. However, apart from the studies of Kretz (1959), Engel & Engel (1960), Krylova *et al.* (1970) and Dahl *et al.* (1993), trace-element thermometry has not been widely tested or applied.

As a result, quantitative understanding of trace-element partitioning and the relative roles of temperature, the major-element composition and crystal structure in determining the distribution coefficients remain rudimentary in metamorphic systems. Available data on trace-element partitioning from natural systems are both scarce and of questionable quality (*e.g.*, DeVore 1955, Turekian & Phinney 1962, Engel & Engel 1960), and experimental data are virtually non-existent because of difficulties in attaining equilibrium. In many of the studies noted above, authors were unable to document systematic trace-element distributions between coexisting metamorphic minerals, possibly because of poor quality of data as well as zoning within one or more of the phases analyzed (especially garnet, *e.g.*, Hickmott *et al.* 1987). The laser-ablation microprobe coupled to an inductively coupled plasma – mass spectrometer (LAM–ICP–MS) holds the promise of changing this situation decisively (Jackson *et al.* 1992, Jenner *et al.* 1993, Fryer *et al.* 1995, Taylor *et al.* 1997) by eliminating uncertainty related to compositional zoning and contamination by solid or fluid micro-inclusions that arise by analyzing mineral separates. However, no applications

of the technique to garnet–biotite pairs have yet been attempted.

In this paper, we provide trace-element data (Sc, Ti, V, Cr, Mn, Co, Ni, Cu, Zn, Nd, Y, Ba, Sr, Zr, Hf, Ta and the rare-earth elements, *REE*) on garnet and biotite from metamorphic rocks equilibrated under greenschist-to upper-amphibolite-facies conditions. Garnet–biotite pairs were chosen for this study because of their widespread coexistence in metapelitic and related rocks, their wide field of stability, from the greenschist to the granulite facies, and their overall utility in petrogenetic studies. In addition, coexisting garnet and biotite provide an independent estimation of metamorphic temperature using conventional major-element thermometry. On the basis of our data and crystal-chemical and thermal considerations, we explore the controls on trace-element partitioning between coexisting garnet and biotite. We believe that the data we have obtained so far add significantly to the current body of knowledge concerning trace-element partitioning between coexisting garnet and biotite.

GEOLOGICAL SETTING

The Grenville Orogen in western Labrador comprises two lithotectonic terranes, the Gagnon and Molson Lake terranes, that are structurally stacked from northwest to southeast on the Ashuanipi Metamorphic Complex foreland of the Superior Province (Fig. 1). Metasedimentary units in the Gagnon terrane, which are part of the Paleoproterozoic Knob Lake Group, experienced a single Barrovian-type regional metamorphism during the Grenvillian Orogeny at *ca.* 1000 Ma (Rivers 1983, Brown *et al.* 1992, van Gool 1992, Rivers *et al.* 1993). During this orogenic event, the Gagnon terrane was incorporated into the base of a major thrust-wedge and was overthrust by the Molson Lake terrane, composed of Late Paleoproterozoic to Mesoproterozoic granitic and gabbroic rocks, from the southeast (Fig. 1).

Rivers (1983) outlined a metamorphic field-gradient from greenschist to upper amphibolite facies in the area, and defined several metamorphic zones on the basis of the following isogradic assemblages of minerals: garnet – biotite (low-T), staurolite – kyanite and kyanite – garnet – biotite (mid-T), and granitic veins (high-T). Pressure – temperature estimates across the

metamorphic field-gradient in the Gagnon terrane indicate an increase in temperature and pressure from *ca.* 435°C and 5.5 kbar in the northwest to 670°C and 11 kbar in the southeast (van Gool 1992), compatible with the variation in mineral assemblages. The presence of relict growth-zoning in some grains of garnet from granitic veins in the highest-grade zone, together with the observation that the P–T paths are hairpin-shaped, suggest that the rocks cooled and were exhumed rapidly, shortly after attaining their peak conditions of metamorphism (van Gool 1992).

Normal patterns of growth zoning are preserved in garnet from garnet – biotite and staurolite – kyanite zones (van Gool 1992). The pattern is characterized by X_{Sps} and X_{Alm} decreasing outward in typical bell-shaped profiles, with X_{Prp} increasing from core to rim. X_{Grs} slightly increases or remains nearly constant from core to rim in garnet from the garnet – biotite zone, and decreases or remains nearly constant in garnet from the higher grades. In the kyanite – garnet – biotite and granitic veins zones, the pattern of growth zoning is perturbed near some garnet rims by an increase in X_{Sps} and X_{Fe} in conjunction with a decrease in X_{Prp}, reflecting the resorption of garnet (van Gool 1992). Flat chemical profiles observed in some cases in garnet from the granitic veins zone indicate homogenization of garnet composition due to intracrystalline diffusion. No breaks in major-element zoning were found, which is consistent with the interpretation of a single episode of prograde metamorphism in the area. Mineral assemblages, textures and
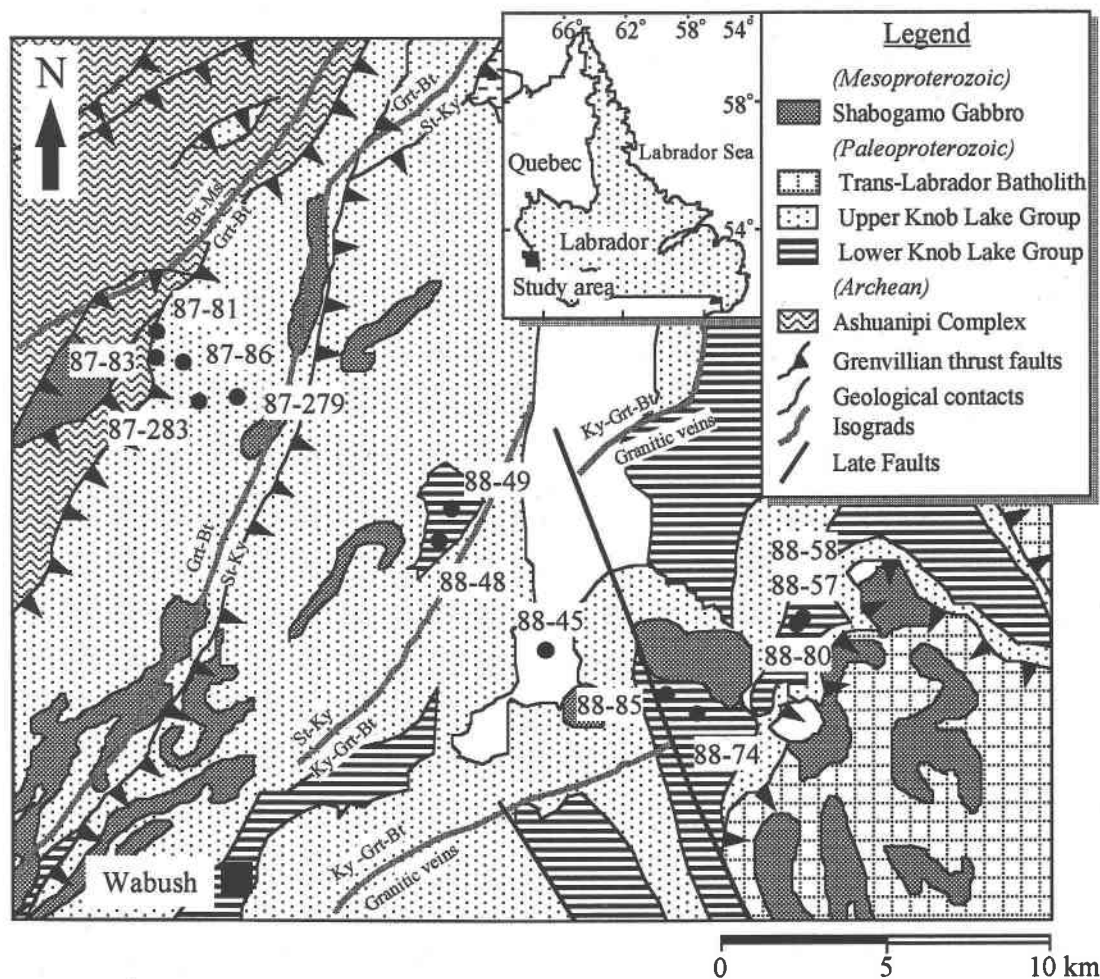

FIG. 1. Generalized geological map of the northern Grenville province in western Labrador, showing metamorphic isograds and locations of the thirteen samples. Geological map and metamorphic isograds from Connelly *et al.* (1996), Rivers (1983) and van Gool (1992).

reactions in metasedimentary rocks from Gagnon terrane are described in detail elsewhere (*e.g.*, Rivers 1983, van Gool 1992).

METHODS AND SAMPLE DESCRIPTION

The thirteen quartzofeldspathic and metapelitic samples chosen for this study include five rocks from the garnet – biotite zone, two from the staurolite – kyanite zone, one from the kyanite – garnet – biotite zone, and five from the granitic veins zone (Fig. 1). Samples from the low-T zone come from the upper Knob Lake Group, whereas those from mid- and high-T zones come from the lower Knob Lake Group. This distinction is significant because the metasedimentary rocks of the upper Knob Lake Group are more Ca-rich than those from the lower Knob Lake Group. Three of the samples from the granitic veins zone (88–80, 88–58 and 88–57) are located very close together and were selected to test for the effects of major-element composition on trace-element partitioning. All selected rocks are composed primarily of quartz, muscovite and biotite, with variable modal proportions of garnet (Table 1). Staurolite occurs only in sample 88–49, which is also characterized by the presence of gedrite. Zircon, apatite, rutile, ilmenite, magnetite, hematite, pyrite, tourmaline, graphite and carbonate occur as accessory minerals in the sample suite.

Muscovite and chlorite occur as minor late-stage minerals, indicating that H_2O-rich fluid has infiltrated the samples. Biotite is typically fresh in appearance, with only local minor chloritization. Garnet growth was largely synkinematic, as grains commonly display sigmoidal internal fabrics. Garnet grains from the garnet – biotite and staurolite – kyanite zones form small (less than about 1 mm in diameter) euhedral or subhedral porphyroblasts that commonly contain abundant inclusions of quartz, apatite, tourmaline, ilmenite and epidote. Although epidote occurs commonly in calcic metapelites in the biotite zone, its occurrence is restricted to inclusions in garnet in the higher-temperature zones. At higher grade, the grains of garnet are large (up to 10 mm in diameter), irregular anhedral porphyroblasts that exhibit evidence of partial resorption during retrograde metamorphism. For garnet showing evidence of resorption, analysis spots were located 50–100 μm away from the rim, the distance being determined from the Mn-zoning profile.

Bulk-rock analysis

For ten samples, concentrations of major elements and first-series transition elements of bulk rocks were determined using a Fisons/ARL® model 8420+ sequential wavelength-dispersion X-ray-fluorescence spectrometer at the Department of Earth Sciences, Memorial University of Newfoundland, as described by Longerich (1995). Samples were prepared as pressed pellets using 5 g of rock powder mixed with 0.7 g of BRP–5933 Bakelite® phenolic resin. Bulk-rock concentrations of 14 rare-earth elements (*REE*) and six other trace-elements (Y, Zr, Nb, Ba, Hf, and Ta) were determined by solution-mode inductively coupled plasma – mass spectrometry (ICP–MS; Perkin Elmer Sciex Elan® model 250) at Memorial University of Newfoundland, following a sodium peroxide (Na_2O_2) sinter digestion procedure (Longerich *et al.* 1990). Synthetic solutions were used to calibrate the ICP–MS. Standard reference materials, MRG–1 and BR–688, and reagent blanks were analyzed for quality-control purposes. Further details of the sample preparation, precision and accuracy are given in Longerich *et al.* (1990).

Micro-analysis

Quantitative analyses of garnet and biotite grains were carried out using a Cameca® SX –50 electron-microprobe analyzer (EMP), in energy-dispersion (EDS) and wavelength-dispersion (WDS) modes at the Department of Earth Sciences, Memorial University of Newfoundland. An accelerating voltage of 15 kV, a beam current of 10 nA and a beam diameter of about 1 to 5 μm were used. Instrument calibration was done on a cobalt standard for EDS analyses and on natural and synthetic standards for WDS analyses, with data reduction of raw counts performed with a Link® ZAF matrix-correction program.

TABLE 1. MINERAL ASSEMBLAGES AND MODAL PERCENTAGES, METAMORPHIC ROCKS FROM WESTERN LABRADOR

Spl.	Qtz	Ms	Bt	Chl	Ep	Pl	Kfs	Ky	Grt	Ged	St	Cal	Tur	Ap	Rt	Zrn	Ilm	Hem	Mag	Py	Gr	Grt/Bt
87-81	41	28	26			<1			<1			<1	<1	<1		<1	<1					0.02
87-83	53	11	28	<1	<1*	<1			4			<1	<1	<1		<1	<1			<1		0.13
87-86	40	11	43	<1	<1*	<1			<1			<1	<1	<1		<1	<1	<1		<1		0.01
87-283	43	<1	45	2†	<1*	<1			<1				<1	<1		<1	<1			<1		0.01
87-279	48	16	23	4†		<1			3			<1		<1		<1	<1			<1	<1	0.11
88-49	27		37	<1†				5	19	2	9		<1		<1*	<1				<1		0.51
88-48	26	10†	44	4		<1		2	10			<1	<1	<1*	<1	<1						0.24
88-45	44	27	11			<1	<1	<1	11					<1*	<1	<1	<1	<1	<1			1.02
88-85	62	29	6			<1		2	<1			<1		<1*	<1	<1			<1	<1		0.12
88-74	34	26	23			2	5	9	<1				<1	<1		<1	<1		<1	<1		0.03
88-80	12	2†	63	2		9		2	4					<1		<1	<1			<1		0.06
88-57	47	<1	37.3	2		6			5							<1	<1			<1		0.14
88-58	34	43	8						11				<1			<1	<1		<1	<1		1.49

* Minerals occur only as inclusions; and † secondary minerals. Mineral abbreviations after Kretz (1983).

Concentrations of trace elements were determined by LAM–ICP–MS at Memorial University of Newfoundland. Current instrumentation and procedures have been described by Taylor *et al.* (1997). A laser sampler utilizing a frequency-quadrupled Nd:YAG laser source with a wavelength of 266 nm was coupled to a Fisons ® –VG PQII+ "S" ICP–MS. The laser was operated in Q-switched mode, with pulse energy optically attenuated to between 0.2 and 0.5 mJ and a pulse-repetition rate of 10 Hz. Calibrations were made against the National Institute of Science and Technology (NIST) standard reference material (SRM) 610, which has a nominal abundance of 500 ppm of the trace elements concerned (Pearce *et al.* 1997). Either Ca (for garnet) or Ti (for biotite), whose concentration was previously determined by EMP analysis, was used as an internal standard to correct for differences in ablation yield between samples and the calibration standard. LAM–ICP–MS analyses were conducted separately for the light (Sc to Ba) and

heavy (*REE* to Ta) elements to increase counting times. Data reduction was performed with an in-house spreadsheet program. From examination of graphical output, the presence of spikes potentially related to ablation of micro-inclusions was assessed, and optimal background and signal time-intervals for integration were selected accordingly. Concentrations and detection limits were calculated using algorithms derived by Longerich *et al.* (1996b).

Given the inherent heterogeneity of minerals and the impossibility of doing repeated measurements on the same spot, the precision of the LAM–ICP–MS technique is difficult to measure on natural samples. However, precision was estimated by repeated analyses of BCR–2G, a glass reference material obtained from the U.S. Geological Survey, using operating conditions similar to those applied during routine analyses (Table 2). The analytical precision for most of the elements is within 10% relative standard deviation (RSD)

TABLE 2. MEAN VALUES, PRECISION AND DETECTION LIMITS
FOR BCR-2G AND SAMPLES

Elements	BCR-2G		Literature values*	Diff. (%)	Detection limits (BCR-2G)			Detection limits (Sample)		
	Mean	Std. dev.			min.	max.	avg.	min.	max.	avg.
Sc	31.5	1.6	32.6	3.49	0.077	11.271	2.608	0.058	216.58	12.53
TiO$_2$	2.04	0.06	2.24	8.99	0.00008	0.00192	0.00033	0.00003	0.05239	0.00216
V	398	16	407	2.16	0.032	1.207	0.233	0.026	22.75	1.64
Cr	15.6	2.3	16	2.29	0.906	25.647	5.058	0.947	416.22	35.00
MnO	0.18	0.01	0.177	3.15	0.000	0.001	0.000	0.000	0.01	0.00
Co	35.4	2.9	37	4.29	0.063	2.103	0.570	0.055	96.02	5.09
Ni	10.6	1.5	13	17.85	0.195	25.662	5.351	0.177	546.72	34.78
Cu	20.7	4.0	19	8.73	0.225	1.228	0.595	0.178	38.73	6.42
Zn	161	15	129.5	24.28	0.152	2.096	1.293	0.153	15.55	3.42
Sr	332	17	337	1.49	0.005	0.057	0.019	0.007	0.52	0.11
Y	31.4	2.6	32.51	3.29	0.003	0.133	0.025	0.003	2.21	0.18
Zr	171	12	184.4	7.53	0.003	0.232	0.046	0.004	7.01	0.31
Nb	9.9	0.9	13.14	24.07	0.002	0.021	0.009	0.003	0.23	0.05
Ba	652	41	681	4.28	0.002	0.480	0.070	0.005	7.89	0.48
La	25.4	1.5	25.3	0.55	0.001	0.039	0.008	0.001	0.86	0.07
Ce	54.8	3.7	53.6	2.22	0.001	0.044	0.007	0.002	0.96	0.06
Pr	7.2	0.4	6.83	4.74	0.001	0.006	0.003	0.001	0.08	0.01
Nd	29.1	1.8	28.63	1.62	0.008	0.252	0.067	0.011	5.62	0.70
Sm	6.7	0.5	6.67	0.71	0.006	0.180	0.042	0.008	3.96	0.38
Eu	2.0	0.2	2	0.59	0.001	0.049	0.011	0.002	0.96	0.11
Gd	6.5	0.5	6.8	5.04	0.006	0.135	0.044	0.008	4.48	0.37
Tb	1.07	0.08	1.04	2.61	0.001	0.004	0.002	0.001	0.06	0.01
Dy	6.6	0.5	6.38	3.89	0.005	0.128	0.026	0.004	2.18	0.22
Ho	1.4	0.1	1.29	6.59	0.001	0.006	0.003	0.001	0.07	0.01
Er	3.8	0.3	3.66	4.23	0.002	0.126	0.028	0.005	2.27	0.23
Tm	0.56	0.05	0.54	3.14	0.001	0.005	0.002	0.001	0.07	0.01
Yb	3.3	0.4	3.34	0.30	0.005	0.206	0.038	0.007	3.46	0.31
Lu	0.50	0.06	0.51	2.22	0.001	0.034	0.009	0.001	0.44	0.05
Hf	5.0	0.6	5.17	4.12	0.004	0.014	0.009	0.009	0.45	0.06
Ta	0.59	0.07	0.78	24.20	0.001	0.002	0.001	0.001	0.22	0.02

All results in ppm, except TiO$_2$ and MnO in wt% oxide. Based on 16 determinations over the period March 19, 1996 to April, 1997. Std. dev. = standard deviation; Diff. = percent difference between literature values and the values from this study for BCR2-G. * Literature values from Govindaraju (1994).

except for Cr, Ni and Cu. For Cr and Ni, concentrations are close to their detection limits (DL; *i.e.* < 4 × DL) as defined by 3σ counting statistic errors (Table 2). For the analyzed minerals, Ni, Cu, Sr, Nb, Ba, La and Ce in garnet, and Ca, Y, Zr, Cu and the heavy rare-earth elements (*HREE*; Ho to Lu) in biotite are near or below detection limits.

Potential sources of error include: (1) inaccuracies in the determination and mismatch of the normalizing elements Ca and Ti by EMP and LAM, (2) contamination from previously ablated grains or micro-inclusions within grains, and (3) fractionation of chalcophile elements such as Zn and Cu during sample ablation and plasma transportation (Longerich *et al.* 1996a). Great efforts were made to spatially match the LAM–ICP–MS and EMP analysis spots to prevent the first error, especially for garnet. However, because of the different sampling resolutions of the two techniques (μm for EMP *versus* tens of μm for LAM–ICP–MS), accuracy can be degraded for minerals that possess significant zoning in the normalizing elements. Detection of inclusions of minerals very different in composition from the host (*e.g.*, apatite or zircon in a silicate) was done by examination of results. However, where silicates are included within silicates containing similar elements, detection of inclusions in the ablated spot is not easy, the only way being the internal consistency of the results. Ba and *HREE* were used as indicators of contamination of garnet and biotite by micro-inclusions and adjacent minerals, respectively. In order to reduce fractionation effects, a sample cell designed to lower the ablation temperature by directing the Ar carrier gas onto the ablation spot in a high-velocity jet was used. The comparable reproducibility of Zn with other elements demonstrates the utility of the sample cell (Table 2). This sample cell also helped to reduce the contamination from adjacent analysis spots, by directing the ablated material away from them. To further reduce within-run fractionation, the laser was operated in defocused mode (*i.e.*, focused ~100 μm above the sample surface), thereby reducing the relative amount of defocusing of the laser beam during ablation. Despite these efforts, however, Cu shows strong fractionation effects, as demonstrated by its low precision for both reference material and samples (Table 2). The pit sizes were generally about 30–60 μm in diameter, depending on target material, length of ablation, pulse energy and degree of defocusing.

RESULTS

Major- and trace-element concentrations

Representative major- and trace-element concentrations in coexisting garnet and biotite from the metasedimentary rocks from western Labrador are presented in Tables 3 and 4, respectively. Corresponding garnet and biotite stoichiometries are given in Tables 5 and 6, respectively, in which cation site-occupancies were assigned on the basis of ionic radii (Shannon 1976).

Garnet is predominantly an almandine–pyrope solid solution (Fig. 2) with X_{Alm} from 0.52 to 0.81 and X_{Prp} from 0.06 to 0.30. X_{Sps} ranges from 0.01 to 0.18; the lowest values are found in the garnet of samples 88–48 and 88–49. X_{Grs} ranges from 0.03 to 0.25, with low values of Ca in high-T garnet except for sample 88–57 (Fig. 2). However, X_{Grs} appears to show no correlation with metamorphic temperature and pressure, and is controlled primarily by differences in bulk composition.

Biotite shows extensive Fe–Mg solid solution; X_{Mg} of biotite ranges from 0.46 to 0.76, with the highest values from sample 88–49, which contains gedrite (Fig. 3). The Al content correlates weakly with the Mg content of biotite, indicating Mg-Tschermaks substitution (Fig. 3). X_K ranges from 0.88 to 0.96 and is mainly controlled by bulk composition (Table 6). The chlorine and fluorine contents of biotite vary between 0.01 and 0.13 wt% and between 0.19 and 0.8 wt%, respectively (Table 4). The Cl- and F-contents of the biotite seem to be independent of the Mg/(Mg + Fe$_{Total}$) value. Biotite from the granitic veins zone is relatively enriched in Ti (Table 6), reflecting the grade-related increase of Ti-saturation in biotite coexisting with ilmenite.

Generally, the concentrations of trace elements in garnet exhibit much greater variation than those in biotite from the same sample (Fig. 4), suggesting that the compositional range in garnet is largely due to trace-element zoning. Garnet is rich in Sc, Mn, Y, Zr and *HREE* compared to coexisting biotite, but has extremely low concentrations of Ni, Cu, Sr, Nb, Ba, Ta and Hf (Fig. 4). The regular and consistent patterns of trace-element distribution, such as for V, Cr, Mn, Co and Zn between coexisting garnet and biotite over a range of concentration and metamorphic grade, suggest equilibration of those elements (Figs. 4c, d, e, f, i). The irregular distribution of Sc between coexisting garnet and biotite in high-T samples (Fig. 4a) can be attributed to resorption of garnet rims because Sc is a strongly "garnet-compatible element". The significant variations of Cr concentration in garnet and biotite are due to its proximity to the limits of detection (Fig. 4d). The abrupt decrease of Zn in garnet and biotite from sample 88–49 is consistent with the coexistence of staurolite in this sample, which is a major carrier of Zn (Fig. 4i). This sample, which is characterized by low Mn and Ca contents, also shows strong depletion in Sc and Y, which are strongly partitioned into garnet (Figs. 4a, k). The whole-rock abundance of Sr, Zr, the light rare-earth elements (*LREE*), Ta and Hf exceeds that measured in any of the analyzed phases (Figs. 4, 5), consistent with their concentration in trace-element-enriched phases such as apatite, zircon, plagioclase, ilmenite and magnetite.

Most whole-rock *REE* patterns in the metasedimentary rocks are similar to those of pelitic sediments

TABLE 3. REPRESENTATIVE COMPOSITIONS OF GARNET, AS DETERMINED BY ELECTRON MICROPROBE AND LAM–ICP–MS

Spl.	87-81		87-83		87-86		87-283		87-279		88-49		88-48		88-45		88-85		88-74		88-80		88-57		88-58	
	F23	G1	C11	C24	C1	C8	C3	D2	D6	D1	A4	A45	D1	D3	E1	E7	C4	D10	C5	D8	B9	B5	A13	A9	B5	C4
(wt%)																										
SiO$_2$	37.50	37.50	37.30	37.10	37.20	37.10	37.10	37.40	37.80	37.80	37.44	37.44	37.20	37.70	37.70	38.00	38.10	38.10	37.30	37.90	39.10	38.90	38.50	38.20	37.90	37.80
TiO$_2$#	0.055	0.048	0.047	0.059	0.031	0.034	0.030	0.063	0.030	0.027	0.010	0.010	0.044	0.065	0.004	0.006	0.005	n.d.	0.005	0.005	0.020	0.004	0.027	0.041	0.003	0.005
Al$_2$O$_3$	21.00	20.80	20.80	21.00	20.70	20.60	20.70	20.90	21.00	21.00	21.48	21.48	21.00	21.10	21.20	21.40	21.30	21.60	21.10	21.20	22.00	22.00	21.30	21.40	21.50	21.30
FeO	30.30	31.60	30.00	30.80	30.10	29.00	27.90	26.90	30.30	30.30	35.94	35.94	35.20	35.40	35.10	35.20	34.90	35.10	35.90	35.30	27.60	28.30	27.20	28.40	38.00	38.30
MgO	1.70	1.90	1.80	1.80	1.70	1.70	1.80	1.60	2.40	2.40	5.70	5.70	4.30	4.20	4.30	4.50	4.40	4.30	3.80	4.00	7.00	6.70	3.40	3.90	3.70	3.70
MnO	3.50	2.70	3.70	4.00	4.30	4.70	3.50	5.10	2.90	2.90	n.d.	n.d.	n.d.	n.d.	0.30	0.30	0.40	0.40	1.90	2.00	3.30	4.90	3.60	2.00	0.40	0.30
CaO	7.30	6.80	7.00	6.40	6.50	6.80	8.70	8.70	6.70	6.70	0.58	0.58	2.30	2.40	2.70	2.80	3.00	3.30	1.60	1.60	3.50	2.10	8.40	7.80	1.60	1.50
Total	101	101	101	101	101	100	100	101	101	101	101	101	100	101	101	102	102	103	102	102	103	103	102	102	103	103
(ppm)																										
Sc	106	102	65	74	63	70	92	135	75		23	n.d.	40	76	83	68	82	93	70	72	176	258	112	64	62	53
V	49	45	68	65	36	47	82	150	144		27	34	44	46	19	22	22	30	17	16	23	25	71	47	19	21
Cr	153	33	34	135	n.d.	84	62	90	79		130	117	305	300	121	164	113	127	85	88	42	239	781	156	209	172
Co	12.9	10.3	16.7	16.4	13.9	14.3	8.2	8.6	6.5		29.6	25.8	20.7	21.5	12.2	10.8	18.5	18.3	37.7	36.4	18.4	16.2	24.3	23.3	19.8	18.7
Ni	n.d.	n.d.	n.d.	n.d.	n.d.	n.d.	n.d.	n.d.	n.d.		n.d.	n.d.	n.d.	94	n.d.	n.d.	n.d.	n.d.	n.d.	n.d.	n.d.	n.d.	n.d.	n.d.	n.d.	n.d.
Cu	n.d.	n.d.	n.d.	n.d.	n.d.	n.d.	n.d.	n.d.	n.d.		n.d.	n.d.	n.d.	n.d.	n.d.	n.d.	n.d.	n.d.	3	3	n.d.	n.d.	n.d.	n.d.	n.d.	n.d.
Zn	46	32	60	64	55	83	68	54	51		6	n.d.	19	23	132	123	115	124	60	62	42	51	68	101	164	161
Sr		n.d.	0.18	n.d.	0.21	0.43	n.d.	n.d.	n.d.		n.d.	n.d.	n.d.	n.d.	n.d.	n.d.	n.d.				n.d.	n.d.	n.d.			
Y	598	357	154	124	706	658	150	372	215		7	4	29	13	450	314	89	103	166	192	95	140	24	58	72	66
Zr	2.2	1.4	1.8	2.1	1.3	1.8	1.0	1.4	1.3	0.9	2.6	2.0	8.1	9.0	1.1	1.7	2.1	2.4	6.0	4.1	16.0	11.4	3.0	2.4	1.0	1.3
Nb	n.d.	n.d.	n.d.	n.d.	n.d.	n.d.	n.d.	n.d.	n.d.				n.d.	n.d.	n.d.	n.d.	n.d.				n.d.	n.d.	n.d.	n.d.		
Ba	n.d.	9.1	2.7	n.d.	0.5	0.2	n.d.	0.2	n.d.	n.d.	n.d.	0.0	n.d.	n.d.	n.d.	n.d.	n.d.	n.d.	n.d.	n.d.	n.d.	n.d.	0.1	n.d.	n.d.	n.d.
La		n.d.	n.d.	n.d.	n.d.	n.d.	0.04	0.03	0.01		n.d.	n.d.	n.d.	0.04	n.d.	0.00	n.d.				n.d.	n.d.	n.d.	n.d.	n.d.	n.d.
Ce		0.07	0.02	0.26	n.d.	n.d.	0.06	0.06	n.d.		n.d.	n.d.	0.03	0.09	n.d.	n.d.	0.00				n.d.	0.00	n.d.	n.d.		
Pr		n.d.	n.d.	n.d.	n.d.	0.00	0.06		0.00		n.d.	n.d.	0.01	0.04	n.d.	0.00	0.09				0.01	0.00	0.01	n.d.	n.d.	n.d.
Nd		n.d.	n.d.	0.24	0.03	n.d.	n.d.		n.d.		n.d.	n.d.	0.29	0.41	n.d.	n.d.	n.d.				0.29	0.14	0.36	0.39	n.d.	n.d.
Sm		n.d.	n.d.	0.21	0.43	n.d.	n.d.		0.32		0.11	0.07	1.55	1.81	0.97	1.00	1.36				1.79	0.95	0.88	0.54		
Eu		0.16	0.18	0.22	0.29	0.24	n.d.	n.d.	0.24		0.08	0.06	0.73	0.43	0.51	0.71	1.05				1.33	0.79	0.93	1.09	0.24	0.25
Gd		1.56	3.02	1.68	3.26	4.39	1.11	1.04	4.22		0.88	0.55	5.60	3.06	12.34	13.79	10.94				11.20	11.63	4.87	5.90		
Tb		1.22	1.66	1.33	2.96	3.36	0.86	1.10	3.16		0.24	0.13	0.91	0.36	6.82	6.13	2.77				3.12	4.01	1.37	1.74	1.37	1.61
Dy		33.9	20.1	15.7	59.0	65.9	16.1	23.3	46.1		1.5	1.0	4.4	2.2	75.9	55.9	13.8				18.9	30.1	7.1	11.3		
Ho		16.98	4.69	3.69	24.80	23.33	6.90	12.75	11.77		0.24	0.19	0.97	0.47	20.81	11.16	1.75				2.78	5.21	0.85	2.37	2.23	2.07
Er		84.19	12.81	10.66	98.09	84.01	27.52	58.34	28.28		0.47	0.43	2.96	1.40	57.33	21.71	3.05				4.84	11.33	1.94	6.33		
Tm		18.10	1.66	1.48	15.80	12.68	4.26	10.06	3.10		0.05	0.03	0.44	0.19	7.04	2.15	0.41				0.43	1.51	0.22	0.94		
Yb		127.6	9.73	8.38	101.3	78.22	25.41	63.74	14.77		0.54	0.23	2.33	1.43	35.77	10.67	2.46				1.84	8.12	1.81	6.68	3.35	3.10
Lu		18.02	1.16	1.17	15.20	11.50	3.50	7.98	1.74		0.11	0.05	0.38	0.23	4.71	1.16	0.36				0.28	1.03	0.28	1.05	0.39	0.52
Hf		n.d.	n.d.	n.d.	n.d.	0.05	n.d.	n.d.	0.02				0.11	0.19	n.d.	0.04	0.02				0.24	0.20				
Ta		n.d.	0.02	0.03	n.d.	n.d.	n.d.	n.d.	n.d.				n.d.	0.00	n.d.	n.d.	n.d.				n.d.	n.d.				

Determined by LAM-ICP-MS. # Total Fe as FeO. n. d. = not detected. Blank = not determined.

worldwide (Taylor & McLennan 1985), being characterized by enriched levels of the *LREE*, depleted levels of *HREE* and negative Eu anomalies, except for samples 88–48 and 88–57 (Fig. 5a). The different *REE* patterns in samples 88–48 and 88–57 are not explained by an unusual mineral assemblage, modal abundance or grain size, features in which they resemble other samples (Table 1). Chondrite-normalized patterns of garnet show a small negative Eu anomaly and marked enrichments in *HREE* relative to *LREE* throughout the metamorphic range (Fig. 5b). The *HREE* are known to be strongly partitioned into garnet during metamorphic crystallization because of their compatibility in the *X*-sites in garnet (Hickmott & Shimizu 1990, Schwandt *et al.* 1993, Ayres & Vance 1994). This effect has resulted in enrichment of *HREE* in some of the garnet rims in samples 88–45, 88–85 and 88–74 during retrograde metamorphism.

Chondrite-normalized *REE* patterns for biotite show *LREE*-enriched profiles with negative Eu anomalies of variable magnitudes with the exception of sample 88–74 (Fig. 5c). Many low-abundance *REE* in biotite have irregular chondrite-normalized patterns because their concentrations approach detection limits. However, most of the *LREE* patterns from La to Gd are consistent and regular. It is encouraging to note the smooth change of *REE* in both garnet and biotite, indicating that the data can be considered valid and permissive of equilibrium.

In summary, the trace-element abundances between coexisting garnet and biotite are attributed primarily to: (1) bulk composition, (2) changing assemblages during prograde metamorphism, as can be seen from Zn concentrations in garnet and biotite from the staurolite – kyanite zone, and (3) retrograde metamorphism, as shown by anomalously high Sc, Y and *HREE* in high-temperature garnet with retrograde rims. Thermal effects on the trace-element concentrations or element ratios in either garnet or biotite were not found.

Partitioning of trace elements

The distribution (*D*) of trace element *i* is defined as the ratio of concentrations (*C*), in ppm:

TABLE 4. REPRESENTATIVE COMPOSITIONS OF BIOTITE, AS DETERMINED BY ELECTRON MICROPROBE AND LAM–ICP–MS

Spl	87-81		87-83		87-86		87-283		87-279		88-49		88-48		88-45		88-85		88-74		88-80		88-57		88-58	
	F8	G12	C23	C9	C34	C4	C5	D5	D3	D3	A5	A1	D2	D4	E2	E4	C5	D11	C6	D9	B4	B6	A12	A12	B3	C3
(wt%)																										
SiO_2	36.7	36.1	37.8	36.5	37.8	36.3	36.9	36.1	37.3	37.3	40.4	40.3	37.6	37.5	37.7	37.3	37.6	37.8	37.0	37.0	38.9	38.1	37.6	37.6	36.9	37.2
TiO_2	1.70	1.60	1.80	1.70	1.70	1.70	1.80	1.80	1.70	1.70	1.40	1.20	1.40	1.40	1.70	1.60	1.70	2.00	2.10	2.20	1.30	1.40	2.00	2.00	2.30	2.20
Al_2O_3	17.2	17.3	18.0	17.1	17.8	17.1	17.4	17.5	17.2	17.2	17.7	17.8	18.7	18.7	18.7	18.6	18.7	18.3	17.8	17.8	19.2	18.7	17.5	17.5	18.1	18.6
FeO^*	20.1	19.7	19.1	20.0	18.8	19.0	19.7	19.7	18.4	18.4	11.6	11.4	15.0	14.6	16.4	16.6	17.7	18.0	12.6	12.8	16.9	16.9			20.4	20.5
MgO	10.0	10.0	11.0	10.5	11.2	10.5	10.7	10.4	11.3	11.3	17.5	17.7	13.4	13.3	12.3	12.3	12.6	12.4	11.7	11.7	15.7	14.9	12.2	12.2	9.7	10.4
$MnO^\#$	0.199	0.149	0.137		0.141	0.138	0.108	0.104	0.176	0.176	n.d.	n.d.	0.005	0.005	0.005	0.005	0.005	0.006	0.030	0.033	0.114	0.095	0.136	0.136	0.023	0.023
Na_2O	n.d.	n.d.	0.20	n.d.	n.d.	n.d.	n.d.	0.30	0.30	0.30	0.80	0.90	0.40	0.50	0.40	0.30	0.50	0.60	0.60	0.80	0.40	0.50	n.d.	n.d.	n.d.	n.d.
K_2O	9.2	9.4	8.9	9.3	9.3	8.8	9.0	9.1	9.1	9.1	8.3	8.4	8.9	8.7	6.9	7.4	8.1	8.0	8.8	8.7	9.0	9.3	9.1	9.1	9.5	9.2
F			0.50		0.50		0.27				0.43	0.20			0.45		0.56		0.33		0.19		0.22	0.22		0.36
Cl			0.04		0.05		0.10				0.04	0.01			n.d.		n.d.		0.02		0.03		0.02	0.02		0.03
Total	95	94	95	95	93	93	95	95	95	95	98	97	95	95	94	94	95	96	96	96	96	96	97	97	97	96
(ppm)																										
Sc	18.5	16.5	12.3		14.9	17.3	16.9	22.3	14.4	14.4	n.d.	n.d.	11.8	12.4	6.3	5.6	4.9	5.4	14.8	15.3	44.4	43.1	43.2	43.2	14.4	13.1
V	191	162	151		174	195	523	550	655	655	305	283	136	125	253	223	261	273	249	261	281	273	485	485	114	108
Cr	173	162	184		147	179	206	184	198	198	366	432	540	422	346	345	306	247	275	338	341	342	685	685	215	172
Co	49.6	39.8	52.4		57.2	57.9	47.3	46.5	19.8	19.8	82.2	79.0	59.8	49.1	25.9	24.5	31.8	36.5	113.9	121.2	42.7	42.4	57.4	57.4	47.1	41.1
Ni	91	99	171		127	132	91	76	39	39	363	352	99	112	72	57	45	44	269	282	143	129	218	218	118	113
Cu	8.4	7.2	7.2		12.0	6.1	10.1	20.5	15.1	15.1	n.d.	5.9	5.2	4.2	22.7	10.4	n.d.	n.d.	n.d.	n.d.	6.2	11.6	n.d.	n.d.	11.9	6.3
Zn	437	278	452		582	617	566	529	647	647	23	16	129	97	843	706	795	902	505	572	271	286	681	681	1196	1017
Sr	1.91	2.42	1.11		1.39	1.50	1.39	1.13	2.00	2.00	22.47	20.65	2.63	2.50	3.15	1.96	4.41	5.89	1.93	2.70	7.99	3.75			4.37	3.70
Y	0.58	1.44	0.70		1.87	0.27	0.92	2.49	1.98	1.98	n.d.	n.d.	n.d.	0.15	0.48	0.18	n.d.	n.d.	n.d.	n.d.	0.05	0.07	n.d.	n.d.	0.09	0.08
Zr	1.32	1.56	0.63		0.52	n.d.	0.98	0.57	0.15	0.15	n.d.	n.d.	0.12	n.d.	0.34	0.10	0.14	0.62	0.10	0.16	0.14	0.14	n.d.	0.09	n.d.	
Nb	47.79	39.67	40.26		49.07	44.84	28.80	23.83	35.23	35.28			26.01	23.03	0.82	0.82	1.01	1.54	17.53	18.63	13.91	12.25				
Ba	1193	905	922	1151	1021	1106	1951	1845	1074	1074	364	304	451	169	637	696	1170	1361	541	665	3084	3046	2597	2597	415	402
La		1.373	0.902	4.331	9.457	9.523	3.890		3.597	3.597	0.020	n.d.	2.109	3.169	1.280	0.749	0.077	0.564	0.056	0.030	0.007	0.136	3.548	3.548	0.133	0.122
Ce		5.21	2.04	5.16	7.69	17.61	9.18		8.87	8.87			3.91	6.87	4.39	2.42	0.17	1.99	0.16	0.09	0.08		4.75	4.75		
Pr		0.538	0.248	1.120	2.363	2.055	1.046		1.508	1.508	0.020	n.d.	0.403	0.713	0.543	0.323	0.025	0.293	0.015	0.010	0.001	0.016	0.701	0.701	n.d.	0.037
Nd		2.43	0.98	4.06	9.27	7.73	4.46		6.28	6.28	n.d.	n.d.	1.33	2.20	2.56	1.27	0.19	1.38	n.d.	0.04	n.d.	0.08	2.71	2.71	0.26	n.d.
Sm		0.45	0.29	0.49	1.85	1.28	0.74		1.10	1.10	n.d.	n.d.	0.07	0.22	0.43	0.24	0.08	0.20	0.01	0.01	n.d.	0.01	0.21	0.21		
Eu		0.104	0.032	0.129	0.180	0.237	0.135		0.186	0.186	n.d.	0.010	0.005	0.020	0.040	0.025	0.022	0.057	0.027	0.010	0.012	0.012	0.089	0.089	n.d.	n.d.
Gd		0.139	0.254	0.425	0.916	0.562	0.852		0.625	0.625	n.d.	n.d.	0.086	0.287	0.166	0.109	0.078	0.048	0.010	n.d.	0.004	n.d.	n.d.			
Tb		0.032	n.d.	0.024	0.066	0.085	0.071		0.080	0.080	0.030	n.d.	n.d.	0.006	0.033	0.019	0.007	0.062	n.d.	n.d.	n.d.	n.d.	n.d.	n.d.	n.d.	
Dy		0.159	n.d.	0.171	0.233	0.459	0.574		0.580	0.580	n.d.	n.d.	0.027	n.d.	0.088	0.054	0.070	0.033	0.030	n.d.	n.d.	n.d.	n.d.	n.d.	n.d.	
Ho		0.046	n.d.	0.045	0.036	0.054	0.096		0.074	0.074	n.d.	n.d.	0.008	n.d.	0.014	0.006	n.d.	n.d.	0.001	n.d.	n.d.	n.d.	n.d.			
Er		0.106	n.d.	0.137	n.d.	0.235	0.377		0.195	0.195	n.d.	n.d.	0.020	0.021	n.d.	n.d.	0.030	n.d.	n.d.	0.003	n.d.	n.d.				
Tm		0.004	n.d.	0.023	n.d.	0.021	0.052		0.033	0.033	n.d.	n.d.	0.006	n.d.	n.d.	n.d.	n.d.	n.d.	n.d.	n.d.	0.006	0.006				
Yb		0.186	0.057	n.d.	n.d.	n.d.	0.185		0.139	0.139	n.d.	n.d.	0.013	n.d.	n.d.	0.019	0.009	0.026	n.d.	n.d.	0.004	n.d.	n.d.	n.d.	n.d.	
Lu		n.d.	0.006	n.d.	0.011	n.d.	0.038		0.025	0.025	n.d.	n.d.	0.002	n.d.	n.d.	n.d.	n.d.	n.d.	n.d.	n.d.	0.002	0.003	n.d.	n.d.	n.d.	n.d.
Hf	0.056	n.d.	n.d.		n.d.	n.d.	0.087		0.018	0.018	n.d.	n.d.	n.d.	n.d.	0.076	n.d.	0.011	0.010	0.020	0.038						
Ta	2.769	2.930	3.513		3.242	1.093	0.776		2.414	2.414			1.054	0.585	0.020	0.024	0.055	0.051	0.970	0.970	0.298	0.242				

\# Determined by LAM–ICP–MS. * Total Fe as FeO. n. d. = not detected. Blank = not determined.

$$D_i = \frac{C_i^{garnet}}{C_i^{biotite}} \tag{1}$$

which is equivalent to the Nernst distribution coefficient. However, a compositional dependence is partly created by the use of D_i, which has only limited thermodynamic significance. In an attempt to eliminate this compositional effect, the term D_i^* was introduced (Nielsen 1985, 1988).

$$D_i^* = \frac{X_i^{garnet}}{X_i^{biotite}} \tag{2}$$

where X is the mole fraction of component i in a specific site in each mineral. Thus, D_i^* depends on the site occupancies of the trace cation in the structures of garnet and biotite. Both D_i and D_i^* are employed in this study. Mole fractions were computed using the stoichiometric data in Tables 5 and 6 on the following basis: three tetrahedrally coordinated sites, two octahedrally coordinated sites and three dodecahedrally coordinated sites for garnet, and two interlayer sites, eight tetrahedrally coordinated sites and six octahedrally coordinated sites for biotite. Ti, V, Cr and Zr are commonly regarded as octahedrally coordinated cations in garnet and biotite, whereas Sc, Co, Zn and *REE* are considered to occupy X sites in garnet (Meagher 1982, Hickmott & Shimizu 1990). In biotite, Sr, Ba and *REE* substitute in the interlayer sites (Dahl *et al.* 1993), and the other trace elements are considered to substitute into the octahedrally coordinated sites on the basis of ionic radius and charges. Vanadium incorporation is dependent on its oxidation state (V^{3+}, V^{4+} or V^{5+}), and the incorporation of Ti in the tetrahedral site cannot definitely be excluded. Calculated D_i^* are listed in Table 7 for representative garnet – biotite pairs, together with estimated metamorphic temperatures using the garnet – biotite geothermometer (Ferry & Spear 1978).

Ti, V, Co, Zn and, to a lesser extent, Cr, are preferentially partitioned into the biotite, whereas Sc, Mn, and in most samples, Sm and Gd are preferentially incorpo-

TABLE 5. STRUCTURAL FORMULA OF REPRESENTATIVE GARNET COMPOSITIONS, EXPRESSED IN CATIONS PER 12 ATOMS OF OXYGEN

Spl.	87-81		87-83		87-86		87-283		87-279		88-49		88-48
	F23	G1	C11	C24	C1	C8	C3	D2	D6	D1	A4	A45	D1
Tetrahedral sites													
Si	2.98	2.98	2.99	2.96	2.99	2.99	2.98	2.98	3.00	3.00	2.95	2.95	2.98
Octahedral sites													
$Ti^{\#}$	3.3E-03	2.9E-03	2.8E-03	3.5E-03	1.9E-03	2.1E-03	1.8E-03	3.8E-03	1.8E-03	1.6E-03	5.9E-04	5.9E-04	2.6E-03
Al	1.97	1.95	1.96	1.98	1.96	1.96	1.96	1.96	1.96	1.96	2.00	2.00	1.98
Fe^{3+}	0.089	0.103	0.086	0.123	0.088	0.075	0.095	0.177	0.058	0.058	0.149	0.149	0.086
V	4.6E-04	4.2E-04	6.4E-04	6.1E-04	3.4E-04	4.4E-04	7.7E-04	1.4E-03	1.3E-03		2.5E-04	3.2E-04	4.2E-04
Cr	1.4E-03	3.0E-04	3.1E-04	1.2E-03	n.d.	7.8E-04	5.8E-04	8.3E-04	7.2E-04		1.2E-03	1.1E-03	2.8E-03
Zr	1.1E-05	7.2E-06	9.3E-06	1.1E-05	7.0E-06	9.6E-06	5.0E-06	7.6E-06	7.0E-06	5.0E-06	1.4E-05	1.0E-05	4.3E-05
Nb	n.d.	n.d.	n.d.	n.d.	n.d.	n.d.	n.d.	n.d.	n.d.				n.d.
Hf		n.d.	n.d.	n.d.	n.d.	1.4E-07	n.d.	n.d.		4.4E-08			3.1E-07
Ta		n.d.	5.6E-08	6.8E-08	n.d.	n.d.	n.d.	n.d.		n.d.			n.d.
Total	2.06	2.06	2.05	2.11	2.05	2.04	2.06	2.14	2.02	2.02	2.15	2.15	2.07
Dodecahedral sites													
Fe^{2+}	1.92	2.00	1.92	1.93	1.93	1.88	1.78	1.61	1.95	1.95	2.37	2.37	2.27
Mg	0.201	0.225	0.215	0.214	0.203	0.204	0.216	0.190	0.284	0.284	0.670	0.670	0.513
Mn	0.236	0.182	0.251	0.271	0.292	0.321	0.238	0.344	0.195	0.195	n.d.	n.d.	n.d.
Ca	0.622	0.580	0.600	0.548	0.559	0.587	0.750	0.742	0.569	0.569	0.049	0.049	0.197
Sc	1.1E-03	1.1E-03	6.9E-04	7.9E-04	6.8E-04	7.6E-04	9.9E-04	1.4E-03	8.0E-04		2.4E-04	n.d.	4.2E-04
Co	1.0E-04	8.4E-05	1.4E-04	1.3E-04	1.1E-04	1.2E-04	6.7E-05	6.9E-05	5.3E-05		2.4E-04	2.1E-04	1.7E-04
Ni	n.d.	n.d.	n.d.	n.d.	n.d.	n.d.	n.d.	n.d.	n.d.		n.d.	n.d.	n.d.
Cu	n.d.	n.d.	n.d.	n.d.	n.d.	n.d.	n.d.	n.d.	n.d.		n.d.	n.d.	n.d.
Zn	3.4E-04	2.4E-04	4.4E-04	4.7E-04	4.0E-04	6.1E-04	5.0E-04	3.9E-04	3.7E-04		4.0E-05	n.d.	1.4E-04
Sr	n.d.	n.d.	n.d.	n.d.	n.d.	n.d.	n.d.	n.d.	n.d.		n.d.		n.d.
Y	3.2E-03	1.9E-03	8.4E-04	6.7E-04	3.8E-03	3.6E-03	8.1E-04	2.0E-03	1.2E-03		3.7E-05	2.0E-05	1.6E-04
Ba	n.d.	3.2E-05	9.5E-06	n.d.	1.9E-06	6.5E-07	n.d.	8.1E-07	n.d.	n.d.	n.d.	1.4E-07	n.d.
La		n.d.	n.d.	n.d.	n.d.	n.d.	1.5E-07	1.0E-07		4.2E-08	n.d.	n.d.	n.d.
Ce		2.5E-07	6.1E-08	9.0E-07	n.d.	n.d.	2.2E-07	2.1E-07		n.d.	n.d.	n.d.	1.1E-07
Pr		n.d.	n.d.	n.d.	n.d.	n.d.	1.5E-08	2.1E-07		5.7E-09	n.d.	n.d.	2.7E-08
Nd		n.d.	n.d.	8.1E-07	1.1E-07	n.d.	n.d.	n.d.		n.d.	n.d.	n.d.	9.7E-07
Sm		n.d.	5.7E-07	n.d.	6.7E-07	1.4E-06	n.d.	n.d.		1.0E-06	3.5E-07	2.2E-07	5.0E-06
Eu		5.1E-07	5.7E-07	7.0E-07	9.1E-07	7.7E-07	n.d.	n.d.		7.5E-07	2.5E-07	1.9E-07	2.3E-06
Gd		4.7E-06	9.2E-06	5.1E-06	1.0E-05	1.4E-05	3.4E-06	3.1E-06		1.3E-05	2.7E-06	1.7E-06	1.7E-05
Tb		3.7E-06	5.0E-06	4.0E-06	9.0E-06	1.0E-05	2.6E-06	3.3E-06		9.5E-06	7.2E-07	3.9E-07	2.8E-06
Dy		1.0E-04	6.0E-05	4.6E-05	1.8E-04	2.0E-04	4.8E-05	6.8E-05		1.4E-04	4.4E-06	2.9E-06	1.3E-05
Ho		4.9E-05	1.4E-05	1.1E-05	7.3E-05	6.9E-05	2.0E-05	3.7E-05		3.4E-05	6.9E-07	5.5E-07	2.8E-06
Er		2.4E-04	3.7E-05	3.1E-05	2.8E-04	2.4E-04	8.0E-05	1.7E-04		8.1E-05	1.3E-06	1.2E-06	8.5E-06
Tm		5.1E-05	4.7E-06	4.2E-06	4.5E-05	3.6E-05	1.2E-05	2.8E-05		8.7E-06	1.4E-07	8.4E-08	1.3E-06
Yb		3.5E-04	2.7E-05	2.3E-05	2.8E-04	2.2E-04	7.1E-05	1.8E-04		4.1E-05	1.5E-06	6.3E-07	6.5E-06
Lu		4.9E-05	3.2E-06	3.2E-06	4.2E-05	3.2E-05	9.7E-06	2.2E-05		4.7E-06	3.0E-07	1.4E-07	1.1E-06
Total	2.99	2.99	2.99	2.97	2.99	3.00	2.99	2.89	3.00	3.00	3.09	3.09	2.98
X_{Mg}	0.09	0.10	0.10	0.10	0.10	0.10	0.11	0.11	0.13	0.13	0.22	0.22	0.18
X_{Alm}	0.65	0.67	0.64	0.65	0.65	0.63	0.60	0.56	0.65	0.65	0.77	0.77	0.76
X_{Prp}	0.07	0.08	0.07	0.07	0.07	0.07	0.07	0.07	0.09	0.09	0.22	0.22	0.17
X_{Sps}	0.08	0.06	0.08	0.09	0.10	0.11	0.08	0.12	0.06	0.06	0.00	0.00	0.00
X_{Grs}	0.21	0.19	0.20	0.18	0.19	0.20	0.25	0.26	0.19	0.19	0.02	0.02	0.07

Notes: Site occupancies were assigned on the basis of ionic radii and charges (Shannon 1976). # Determined by LAM-ICP-MS. n.d. = not detected. Blank = not determined. X_{Mg}=Mg/(Mg+Fe); X_{Alm}=Fe/(Fe+Mg+Mn+Ca); X_{Prp}=Mg/(Fe+Mg+Mn+Ca); X_{Sps}=Mn/(Fe+Mg+Mn+Ca); X_{Grs}=Ca/(Fe+Mg+Mn+Ca).

TABLE 5 (cont'd). STRUCTURAL FORMULA OF REPRESENTATIVE GARNET COMPOSITIONS, EXPRESSED IN CATIONS PER 12 ATOMS OF OXYGEN

Spl.	88-48	88-45		88-85		88-74		88-80		88-57		88-58	
	D3	E1	E7	C4	D10	C5	D8	B9	B5	A13	A9	B5	C4
Tetrahedral sites													
Si	2.99	2.98	2.97	2.98	2.97	2.96	2.99	2.98	2.98	2.99	2.98	2.97	2.97
Octahedral sites													
Ti[#]	3.9E-03	2.2E-04	3.3E-04	3.0E-04	n.d.	3.1E-04	2.9E-04	1.1E-03	2.2E-04	1.6E-03	2.4E-03	1.9E-04	2.7E-04
Al	1.97	1.97	1.97	1.97	1.98	1.98	1.97	1.98	1.98	1.95	1.97	1.98	1.97
Fe^{3+}	0.056	0.096	0.110	0.094	0.120	0.136	0.078	0.072	0.088	0.105	0.108	0.114	0.127
V	4.3E-04	1.8E-04	2.0E-04	2.0E-04	2.8E-04	1.6E-04	1.5E-04	2.1E-04	2.2E-04	6.5E-04	4.3E-04	1.7E-04	1.9E-04
Cr	2.7E-03	1.1E-03	1.5E-03	1.0E-03	1.1E-03	7.8E-04	8.0E-04	3.7E-04	2.1E-03	7.0E-03	1.4E-03	1.9E-03	1.6E-03
Zr	4.7E-05	5.5E-06	8.8E-06	1.1E-05	1.2E-05	3.2E-05	2.1E-05	8.0E-05	5.7E-05	1.5E-05	1.2E-05	5.1E-06	6.8E-06
Nb	n.d.	n.d.	n.d.	n.d.	n.d.	n.d.	n.d.	n.d.	n.d.				
Hf	5.2E-07	n.d.	9.4E-08	4.9E-08				6.2E-07	5.3E-07				
Ta	5.9E-09	n.d.	n.d.	n.d.				n.d.	n.d.				
Total	2.03	2.07	2.09	2.06	2.10	2.11	2.05	2.05	2.07	2.06	2.08	2.10	2.10
Dodecahedral sites													
Fe^{2+}	2.29	2.22	2.19	2.19	2.17	2.25	2.25	1.69	1.72	1.66	1.74	2.37	2.39
Mg	0.496	0.506	0.525	0.514	0.499	0.450	0.470	0.796	0.764	0.393	0.453	0.432	0.433
Mn	n.d.	0.020	0.020	0.027	0.026	0.128	0.134	0.213	0.317	0.236	0.132	0.027	0.020
Ca	0.204	0.229	0.235	0.252	0.275	0.136	0.135	0.286	0.172	0.698	0.651	0.134	0.126
Sc	8.1E-04	8.8E-04	7.1E-04	8.6E-04	9.7E-04	7.5E-04	7.6E-04	1.8E-03	2.6E-03	1.2E-03	6.7E-04	6.5E-04	5.5E-04
Co	1.7E-04	9.8E-05	8.6E-05	1.5E-04	1.5E-04	3.1E-04	2.9E-04	1.4E-04	1.3E-04	1.9E-04	1.8E-04	1.6E-04	1.5E-04
Ni	7.6E-04	n.d.	n.d.	n.d.	n.d.	n.d.	n.d.	n.d.	n.d.	n.d.	n.d.	n.d.	n.d.
Cu	n.d.	n.d.	n.d.	n.d.	n.d.	n.d.	n.d.	2.4E-05	2.1E-05	n.d.	n.d.	n.d.	n.d.
Zn	1.7E-04	9.6E-04	8.8E-04	8.3E-04	8.9E-04	4.4E-04	4.5E-04	3.0E-04	3.6E-04	4.8E-04	7.3E-04	1.2E-03	1.2E-03
Sr	n.d.	n.d.	n.d.	n.d.	n.d.	n.d.	n.d.	n.d.	n.d.			5.0E-07	n.d.
Y	7.1E-05	2.4E-03	1.7E-03	4.7E-04	5.4E-04	8.9E-04	1.0E-03	4.9E-04	7.2E-04	1.2E-04	3.1E-04	3.8E-04	3.5E-04
Ba	n.d.	n.d.	n.d.	n.d.	n.d.	n.d.	n.d.	n.d.	n.d.	1.9E-07	n.d.	n.d.	n.d.
La	1.3E-07	n.d.	1.2E-08	n.d.				n.d.	n.d.	n.d.	n.d.	n.d.	n.d.
Ce	3.0E-07	n.d.	n.d.	9.8E-09				n.d.	6.0E-09	n.d.	n.d.		
Pr	1.4E-07	n.d.	1.6E-08	2.9E-07				3.3E-08	4.9E-09	3.9E-08	n.d.	n.d.	n.d.
Nd	1.4E-06	n.d.	n.d.	n.d.				9.2E-07	4.5E-07	1.2E-06	1.3E-06	n.d.	n.d.
Sm	5.7E-06	3.1E-06	3.1E-06	4.3E-06				5.5E-06	2.9E-06	2.7E-06	1.7E-06		
Eu	1.4E-06	1.6E-06	2.2E-06	3.3E-06				4.0E-06	2.4E-06	2.8E-06	3.4E-06	7.5E-07	7.6E-07
Gd	9.3E-06	3.7E-05	4.1E-05	3.3E-05				3.3E-05	3.4E-05	1.4E-05	1.8E-05		
Tb	1.1E-06	2.0E-05	1.8E-05	8.2E-06				9.0E-06	1.2E-05	4.0E-06	5.1E-06	4.0E-06	4.8E-06
Dy	6.4E-06	2.2E-04	1.6E-04	4.0E-05				5.3E-05	8.5E-05	2.0E-05	3.3E-05		
Ho	1.4E-06	6.0E-05	3.2E-05	5.0E-06				7.7E-06	1.5E-05	2.4E-06	6.7E-06	6.4E-06	5.9E-06
Er	4.0E-06	1.6E-04	6.1E-05	8.6E-06				1.3E-05	3.1E-05	5.4E-06	1.8E-05		
Tm	5.4E-07	2.0E-05	6.0E-06	1.1E-06				1.2E-06	4.1E-06	6.0E-07	2.6E-06		
Yb	3.9E-06	9.8E-05	2.9E-05	6.7E-06				4.9E-06	2.2E-05	4.9E-06	1.8E-05	9.1E-06	8.5E-06
Lu	6.2E-07	1.3E-05	3.1E-06	9.8E-07				7.3E-07	2.7E-06	7.4E-07	2.8E-06	1.1E-06	1.4E-06
Total	2.99	2.98	2.98	2.99	2.97	2.97	2.99	2.99	2.98	2.99	2.98	2.97	2.97
X_{Mg}	0.18	0.19	0.19	0.19	0.19	0.17	0.17	0.32	0.31	0.19	0.21	0.15	0.15
X_{Alm}	0.77	0.75	0.74	0.73	0.73	0.76	0.75	0.57	0.58	0.56	0.58	0.80	0.80
X_{Prp}	0.17	0.17	0.18	0.17	0.17	0.15	0.16	0.27	0.26	0.13	0.15	0.15	0.15
X_{Sps}	0.00	0.01	0.01	0.01	0.01	0.04	0.04	0.07	0.11	0.08	0.04	0.01	0.01
X_{Grs}	0.07	0.08	0.08	0.08	0.09	0.05	0.05	0.10	0.06	0.23	0.22	0.05	0.04

Notes: Site occupancies were assigned on the basis of ionic radii and charges (Shannon 1976). [#] Determined by LAM-ICP-MS. n.d. = not detected. Blank = not determined. X_{Mg}=Mg/(Mg+Fe); X_{Alm}=Fe/(Fe+Mg+Mn+Ca); X_{Prp}=Mg/(Fe+Mg+Mn+Ca); X_{Sps}=Mn/(Fe+Mg+Mn+Ca); X_{Grs}=Ca/(Fe+Mg+Mn+Ca).

TABLE 6. STRUCTURAL FORMULA OF REPRESENTATIVE BIOTITE COMPOSITIONS, EXPRESSED IN CATIONS PER 22 ATOMS OF OXYGEN

Spl.	87-81		87-83		87-86		87-283		87-279		88-49		88-48
	F8	G12	C23	C9	C34	C4	C5	D5	D3	D3	A5	A1	D2
Tetrahedral sites													
Si	5.60	5.56	5.62	5.57	5.65	5.59	5.57	5.50	5.61	5.61	5.69	5.71	5.55
Al^{iv}	2.40	2.44	2.38	2.43	2.35	2.41	2.43	2.50	2.39	2.39	2.31	2.29	2.45
Octahedral sites													
Ti	0.195	0.185	0.201	0.195	0.191	0.197	0.204	0.206	0.192	0.192	0.148	0.128	0.155
Al^{vi}	0.686	0.700	0.782	0.646	0.788	0.694	0.661	0.649	0.656	0.656	0.626	0.680	0.798
Fe	2.56	2.54	2.38	2.55	2.35	2.45	2.49	2.51	2.31	2.31	1.37	1.35	1.85
Mg	2.27	2.30	2.44	2.39	2.50	2.41	2.41	2.36	2.53	2.53	3.67	3.74	2.95
$Mn^{\#}$	2.6E-02	1.9E-02	2.5E-02	n.d.	n.d.	1.8E-02	1.4E-02	1.3E-02	2.2E-02	2.2E-02	n.d.	n.d.	5.7E-04
Sc	3.8E-04	3.4E-04	2.5E-04		3.1E-04	3.6E-04	3.4E-04	4.5E-04	2.9E-04	2.9E-04	n.d.	n.d.	2.3E-04
V	3.4E-03	2.9E-03	2.7E-03		3.2E-03	3.5E-03	9.3E-03	9.9E-03	1.2E-02	1.2E-02	5.1E-03	4.7E-03	2.4E-03
Cr	3.0E-03	2.9E-03	3.2E-03		2.6E-03	3.2E-03	3.6E-03	3.2E-03	3.4E-03	3.4E-03	6.0E-03	7.1E-03	9.2E-03
Co	7.7E-04	6.2E-04	8.1E-04		9.0E-04	9.1E-04	7.3E-04	7.2E-04	3.0E-04	3.0E-04	1.2E-03	1.1E-03	9.0E-04
Ni	1.4E-03	1.6E-03	2.6E-03		2.0E-03	2.1E-03	1.4E-03	1.2E-03	6.1E-04	6.1E-04	5.2E-03	5.1E-03	1.5E-03
Cu	1.2E-04	1.1E-04	1.0E-04		1.8E-04	8.9E-05	1.4E-04	3.0E-04	2.1E-04	2.1E-04	n.d.	8.0E-05	7.3E-05
Zn	6.1E-03	3.9E-03	6.3E-03		8.2E-03	8.7E-03	7.8E-03	7.4E-03	8.9E-03	8.9E-03	3.0E-04	2.1E-04	1.7E-03
Y	5.9E-06	1.5E-05	7.1E-06		1.9E-05	2.8E-06	9.4E-06	2.6E-05	2.0E-05	2.0E-05	n.d.	n.d.	n.d.
Zr	1.3E-05	1.6E-05	6.3E-06	5.3E-06	n.d.	n.d.	9.8E-06	5.8E-06	1.5E-06	1.5E-06	n.d.	n.d.	1.2E-06
Nb	4.7E-04	4.0E-04	3.9E-04		4.9E-04	4.5E-04	2.8E-04	2.4E-04	3.4E-04	3.4E-04			2.5E-04
Hf		2.9E-07	n.d.	n.d.	n.d.		n.d.	4.5E-07	9.0E-08	9.0E-08			n.d.
Ta		1.4E-05	1.5E-05	1.8E-05	1.7E-05		5.5E-06	3.9E-06	1.2E-05	1.2E-05			5.2E-06
Total	5.76	5.75	5.84	5.78	5.84	5.79	5.80	5.77	5.74	5.74	5.83	5.91	5.77
X_{Mg}	0.47	0.48	0.51	0.48	0.52	0.50	0.49	0.48	0.52	0.52	0.73	0.73	0.61
Interlayer sites													
Na	n.d.	n.d.	0.058	n.d.	n.d.	n.d.	n.d.	0.089	0.087	0.087	0.218	0.247	0.114
K	1.79	1.85	1.69	1.81	1.77	1.73	1.73	1.77	1.75	1.75	1.49	1.52	1.68
F			0.235		0.236							0.193	
Cl			0.010		0.013							0.010	
Sr	2.0E-05	2.6E-05	1.1E-05		1.5E-05	1.6E-05	1.4E-05	1.2E-05	2.1E-05	2.1E-05	2.2E-04	2.0E-04	2.7E-05
Ba	8.0E-03	6.1E-03	6.1E-03	7.7E-03	6.9E-03	7.5E-03	1.3E-02	1.2E-02	7.1E-03	7.1E-03	2.2E-03	1.9E-03	2.9E-03
La		9.1E-06	5.9E-06	2.9E-05	6.3E-05		6.2E-05	2.6E-05	2.3E-05	2.3E-05	1.2E-07	n.d.	1.3E-05
Ce		3.4E-05	1.3E-05	3.4E-05	5.1E-05		1.1E-04	6.0E-05	5.7E-05	5.7E-05	n.d.	n.d.	2.5E-05
Pr		3.5E-06	1.6E-06	7.3E-06	1.6E-05		1.3E-05	6.8E-06	9.7E-06	9.7E-06	1.2E-07	n.d.	2.5E-06
Nd		1.6E-05	6.2E-06	2.6E-05	6.0E-05		4.9E-05	2.8E-05	3.9E-05	3.9E-05	n.d.	n.d.	8.2E-06
Sm		2.8E-06	1.8E-06	3.0E-06	1.1E-05		7.7E-06	4.5E-06	6.6E-06	6.6E-06	n.d.	n.d.	4.0E-07
Eu		6.4E-07	1.9E-07	7.8E-07	1.1E-06		1.4E-06	8.1E-07	1.1E-06	1.1E-06	n.d.	5.6E-08	2.8E-06
Gd		8.2E-06	1.5E-06	2.5E-06	5.4E-06		3.2E-06	5.0E-06	3.6E-06	3.6E-06	n.d.	n.d.	n.d.
Tb		1.8E-06	n.d.	1.4E-07	3.8E-07		4.8E-07	4.1E-07	4.5E-07	4.5E-07	1.6E-07	n.d.	n.d.
Dy		9.0E-07	n.d.	9.6E-07	1.3E-06		2.6E-06	3.2E-06	3.2E-06	3.2E-06	n.d.	n.d.	1.5E-07
Ho		2.6E-07	n.d.	2.5E-07	2.0E-07		3.0E-07	5.4E-07	4.1E-07	4.1E-07	n.d.	n.d.	n.d.
Er		5.9E-07	n.d.	7.5E-07			1.3E-06	2.1E-06	1.1E-06	1.1E-06	n.d.	n.d.	n.d.
Tm		2.1E-08	n.d.	1.2E-07			1.1E-07	2.8E-07	1.8E-07	1.8E-07	n.d.	n.d.	3.4E-08
Yb		1.0E-06	3.0E-07	n.d.	n.d.		n.d.	9.8E-07	7.2E-07	7.2E-07	n.d.	n.d.	6.9E-08
Lu		n.d.	3.2E-08	n.d.	5.9E-08		n.d.	2.0E-07	1.3E-07	1.3E-07	n.d.	n.d.	1.2E-08
Total	1.80	1.85	2.00	1.82	2.03	1.74	1.75	1.87	1.84	1.84	1.71	1.97	1.79
X_K	1.00	1.00	0.97	1.00	1.00	1.00	1.00	0.95	0.95	0.95	0.87	0.86	0.94

Site occupancies were assigned on the basis of ionic radii and charges (Shannon 1976). [#] determined by LAM-ICP-MS. n.d. = not detected. Blank = not determined. X_{Mg}=Mg/(Mg+Fe); X_K=K/(K+Na).

TABLE 6 (cont'd). STRUCTURAL FORMULA OF REPRESENTATIVE BIOTITE COMPOSITIONS, EXPRESSED IN CATIONS PER 22 ATOMS OF OXYGEN

Spl.	88-48	88-45		88-85		88-74		88-80		88-57		88-58	
	D4	E2	E4	C5	D11	C6	D9	B4	B6	A12	A12	B3	C3
Tetrahedral sites													
Si	5.56	5.61	5.58	5.54	5.57	5.53	5.51	5.58	5.55	5.63	5.63	5.52	5.50
Al^{iv}	2.44	2.39	2.42	2.46	2.43	2.47	2.49	2.42	2.45	2.37	2.37	2.48	2.50
Octahedral sites													
Ti	0.156	0.190	0.180	0.189	0.222	0.236	0.246	0.140	0.153	0.225	0.225	0.259	0.245
Al^{vi}	0.828	0.890	0.853	0.794	0.750	0.660	0.627	0.822	0.758	0.720	0.720	0.711	0.735
Fe	1.81	2.00	2.05	2.02	2.05	2.21	2.24	1.51	1.56	2.12	2.12	2.55	2.53
Mg	2.94	2.73	2.74	2.77	2.72	2.60	2.59	3.36	3.23	2.72	2.72	2.16	2.29
$Mn^{\#}$	6.6E-04	5.7E-04	6.1E-04	6.6E-04	7.6E-04	3.7E-03	4.2E-03	n.d.	1.2E-02	n.d.		n.d. 3.0E-03	n.d.
Sc	2.5E-04	1.3E-04	1.1E-04	9.6E-05	1.1E-04	3.0E-04	3.0E-04	8.6E-04	8.4E-04	8.6E-04	8.6E-04	2.9E-04	2.7E-04
V	2.2E-03	4.4E-03	3.9E-03	4.5E-03	4.7E-03	4.4E-03	4.6E-03	4.8E-03	4.7E-03	8.5E-03	8.5E-03	2.0E-03	1.9E-03
Cr	7.2E-03	5.9E-03	6.0E-03	5.2E-03	4.2E-03	4.7E-03	5.8E-03	5.7E-03	5.8E-03	1.2E-02	1.2E-02	3.7E-03	3.0E-03
Co	7.4E-04	3.9E-04	3.7E-04	4.8E-04	5.5E-04	1.7E-03	1.8E-03	6.3E-04	6.3E-04	8.7E-04	8.7E-04	7.2E-04	6.3E-04
Ni	1.7E-03	1.1E-03	8.7E-04	6.7E-04	6.7E-04	4.1E-03	4.3E-03	2.1E-03	1.9E-03	3.3E-03	3.3E-03	1.8E-03	1.7E-03
Cu	5.9E-05	3.2E-04	1.5E-04	n.d.	n.d.	n.d.	n.d.	8.5E-05	1.6E-04	n.d.		n.d. 1.7E-04	9.0E-05
Zn	1.3E-03	1.2E-02	9.7E-03	1.1E-02	1.2E-02	6.9E-03	7.8E-03	3.6E-03	3.8E-03	9.3E-03	9.3E-03	1.6E-02	1.4E-02
Y	1.5E-06	4.8E-06	1.8E-06	n.d.	n.d.	n.d.	n.d.	4.9E-07	7.3E-07	n.d.		n.d. 9.1E-07	8.3E-07
Zr	n.d.	3.3E-06	1.0E-06	1.4E-06	6.0E-06	1.0E-06	1.6E-06	1.4E-06	1.4E-06	n.d.		n.d. 8.7E-07	n.d.
Nb	2.2E-04	7.9E-06	7.9E-06	9.6E-06	1.5E-05	1.7E-04	1.8E-04	1.3E-04	1.2E-04				
Hf	n.d.	n.d.	n.d.	3.8E-07	n.d.	5.7E-08	5.0E-08	9.7E-08	1.9E-07				
Ta	2.9E-06	9.7E-08	1.2E-07	2.7E-07	2.5E-07	4.8E-06	4.8E-06	1.4E-06	1.2E-06				
Total	5.75	5.84	5.85	5.80	5.77	5.74	5.74	5.85	5.73	5.82	5.82	5.71	5.83
X_{Mg}	0.62	0.58	0.57	0.58	0.57	0.54	0.54	0.69	0.67	0.56	0.56	0.46	0.47
Interlayer sites													
Na	0.144	0.115	0.087	0.143	0.171	0.174	0.231	0.111	0.141	n.d.	n.d.	n.d.	n.d.
K	1.65	1.31	1.41	1.52	1.50	1.68	1.65	1.65	1.73	1.74	1.74	1.81	1.73
F								0.086		0.104	0.104		0.168
Cl								0.007		0.005	0.005		0.008
Sr	2.5E-05	3.2E-05	2.0E-05	4.5E-05	6.0E-05	2.0E-05	2.8E-05	7.9E-05	3.7E-05	n.d.		n.d. 4.5E-05	3.8E-05
Ba	1.1E-03	4.1E-03	4.6E-03	7.5E-03	8.8E-03	3.5E-03	4.3E-03	2.0E-02	1.9E-02	1.7E-02	1.7E-02	2.7E-03	2.7E-03
La	2.0E-05	8.2E-06	4.8E-06	4.9E-07	3.6E-06	3.6E-07	1.9E-07	4.5E-08	8.6E-07	2.3E-05	2.3E-05	8.6E-07	7.9E-07
Ce	4.4E-05	2.8E-05	1.6E-05	1.1E-06	1.3E-05	1.1E-06	5.7E-07	n.d.	5.3E-07	3.0E-05	3.0E-05		
Pr	4.5E-06	3.4E-06	2.1E-06	1.6E-07	1.8E-06	9.2E-08	6.3E-08	3.7E-09	1.0E-07	4.4E-06	4.4E-06	n.d.	2.4E-07
Nd	1.4E-05	1.9E-06	7.9E-06	1.2E-06	8.5E-06	n.d.	2.5E-07	n.d.	5.1E-07	1.7E-05	1.7E-05	1.6E-06	n.d.
Sm	1.3E-06	2.5E-06	1.4E-06	4.5E-07	1.2E-06	3.3E-08	5.9E-08	n.d.	7.0E-08	1.2E-06	1.2E-06		
Eu	1.2E-07	2.3E-07	1.5E-07	1.3E-07	3.3E-07	1.6E-07	5.9E-08	6.9E-08	6.6E-08	5.2E-07	5.2E-07	n.d.	n.d.
Gd	4.9E-07	1.6E-06	9.5E-07	6.1E-07	4.4E-07	2.8E-07	5.7E-08	n.d.	2.2E-08	n.d.	n.d.		
Tb	3.3E-08	1.9E-07	1.1E-07	4.0E-08	3.4E-07	n.d.	n.d.	n.d.	n.d.	n.d.	n.d.	n.d.	n.d.
Dy	n.d.	4.9E-07	3.0E-07	3.8E-07	1.8E-07	1.7E-07	n.d.	n.d.	n.d.	n.d.	n.d.		
Ho	n.d.	4.1E-08	n.d.	7.7E-08	3.4E-08	n.d.	n.d.	n.d.	7.2E-09	n.d.	n.d.	n.d.	n.d.
Er	1.1E-07	1.1E-07	n.d.	n.d.	n.d.	1.6E-07	n.d.	n.d.	1.6E-08	n.d.	n.d.		
Tm	n.d.	n.d.	n.d.	n.d.	n.d.	4.8E-09	n.d.	n.d.	n.d.	3.0E-08	3.0E-08		
Yb	n.d.	n.d.	1.0E-07	4.4E-08	1.3E-07	n.d.	n.d.	2.2E-08	n.d.	n.d.	n.d.	n.d.	n.d.
Lu	n.d.	n.d.	n.d.	n.d.	n.d.	n.d.	n.d.	1.1E-08	1.8E-08	n.d.	n.d.	n.d.	n.d.
Total	1.79	1.43	1.50	1.67	1.68	1.85	1.89	1.87	1.89	1.86	1.86	1.82	1.91
X_K	0.92	0.92	0.94	0.91	0.90	0.91	0.88	0.94	0.92	1.00	1.00	1.00	1.00

Site occupancies were assigned on the basis of ionic radii and charges (Shannon 1976). $^{\#}$ determined by LAM-ICP-MS. n.d. = not detected. Blank = not determined. $X_{Mg}=Mg/(Mg+Fe)$; $X_K=K/(K+Na)$.
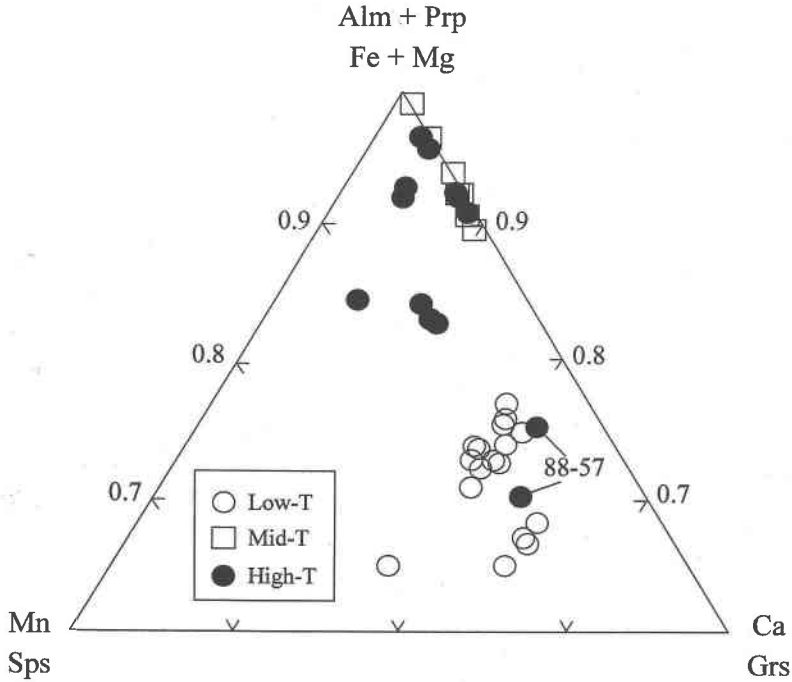
FIG. 2.   Garnet compositions on the basis of dodecahedrally coordinated Fe, Mg, Mn and Ca. Note that the low-temperature samples are more Ca-rich.
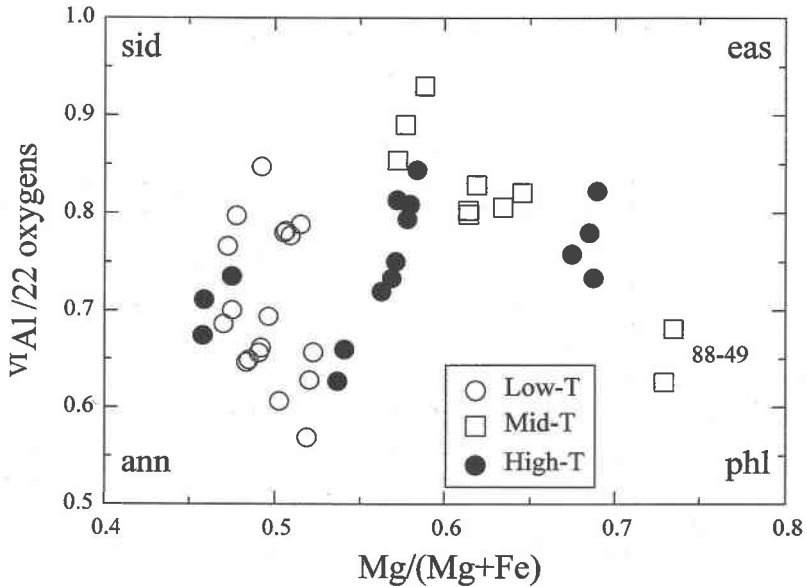

FIG. 3.   Biotite compositions in the idealized annite – phlogopite – siderophyllite – eastonite plane, assuming all iron as ferrous. Sample 88–49 containing gedrite shows the highest value of X_{Mg}. Symbols: sid siderophyllite, eas eastonite, ann annite, phl phlogopite.
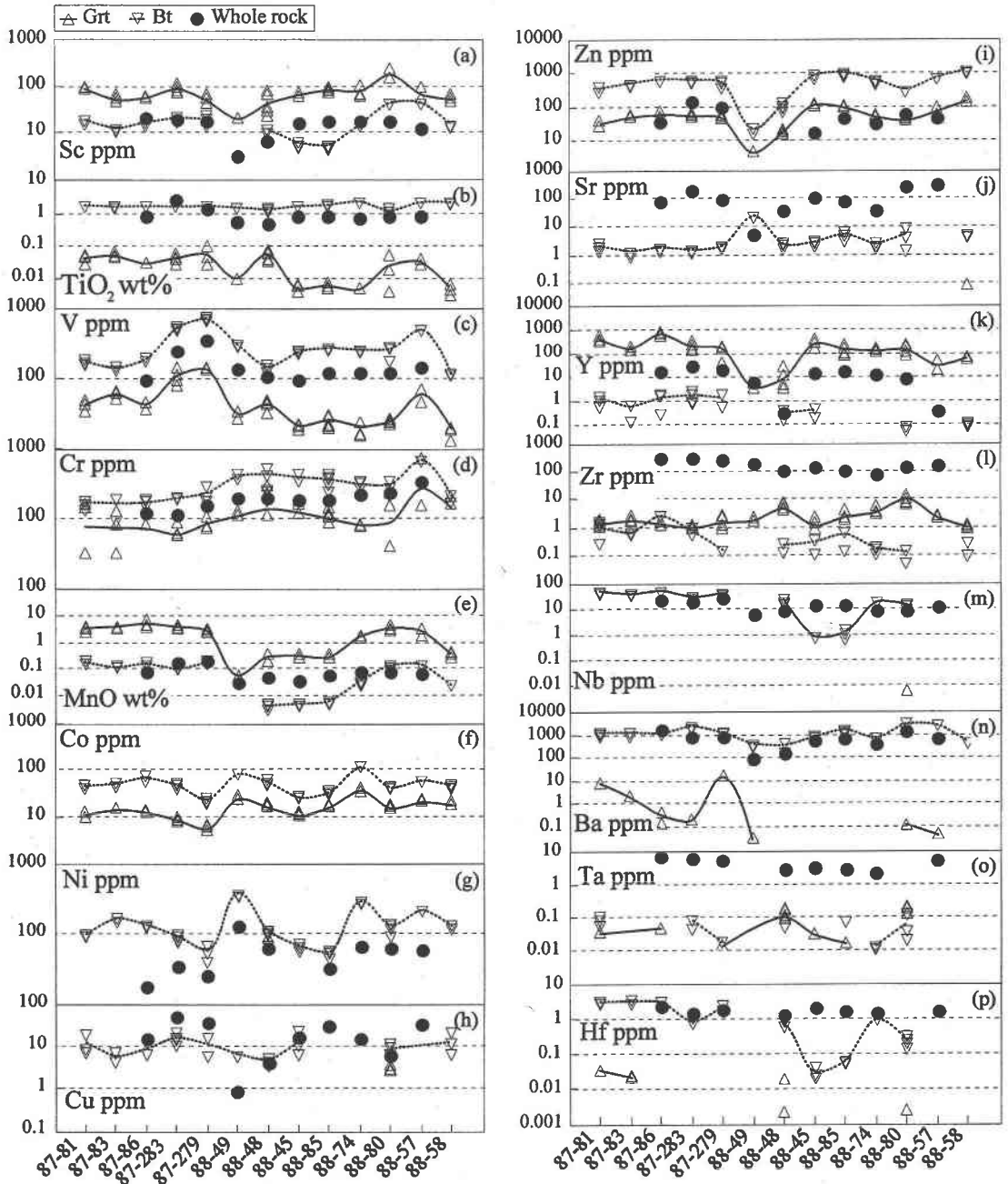
FIG. 4. Trace-element concentrations in garnet, biotite and whole rock. Samples are arranged in the order of increasing meta-morphic grade. Solid and dotted lines represent garnet and biotite, respectively. The within-sample compositional change of garnet and biotite is shown by multiple symbols, each representing a single analysis. Note the systematic variations of V, Cr, Mn, Co and Zn concentrations in garnet and biotite over the range of temperature and bulk composition and the abrupt depletion of Zn concentration in sample 88–49 from the staurolite zone.
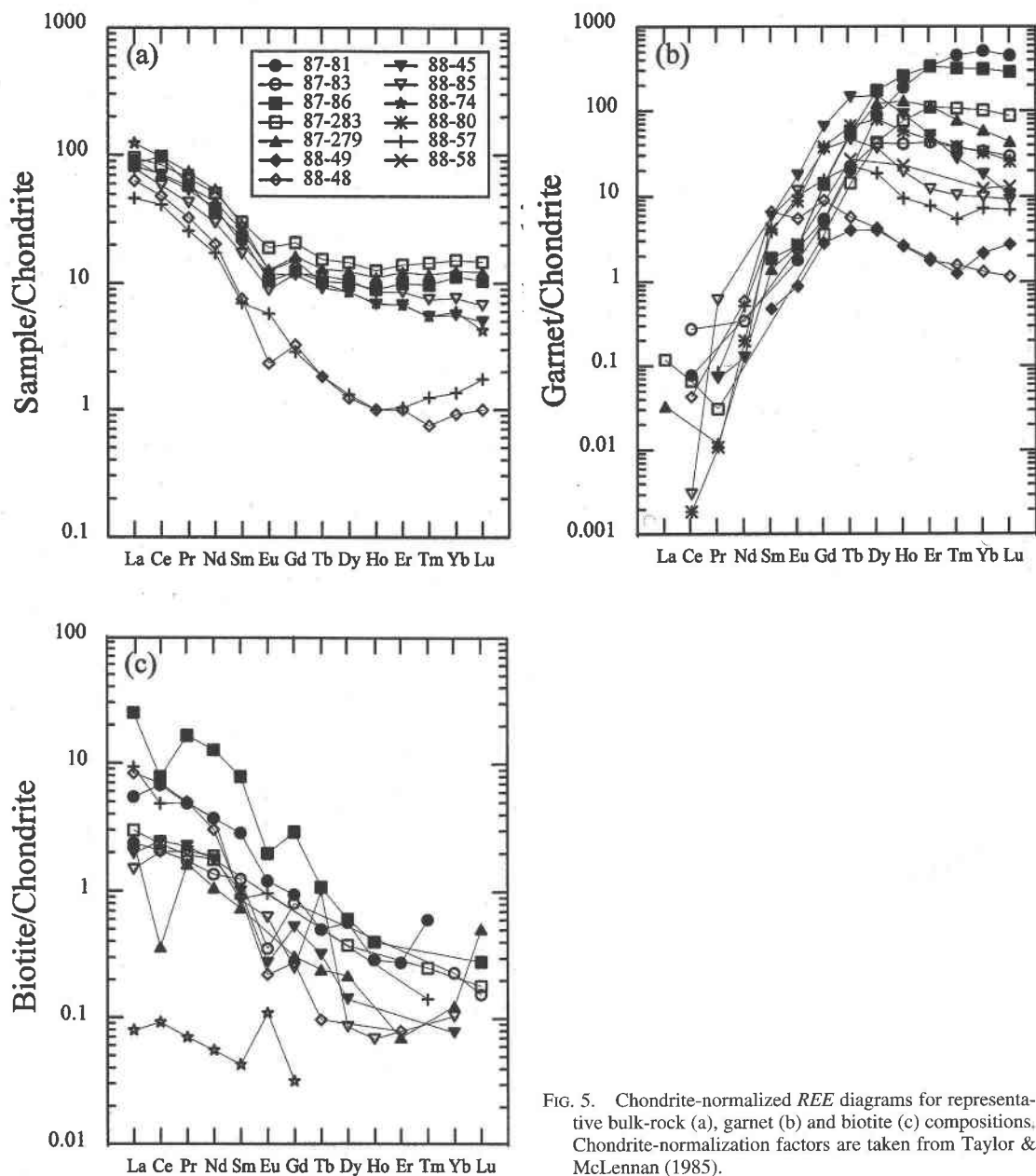
FIG. 5. Chondrite-normalized *REE* diagrams for representative bulk-rock (a), garnet (b) and biotite (c) compositions. Chondrite-normalization factors are taken from Taylor & McLennan (1985).

rated into garnet (Figs. 6a–i). The analytical uncertainties shown in Figure 6 are given as 1σ standard deviations measured from the counting statistics on the background, integrated signals of analyte and the elements used as an internal standard for sample and standard. The broad fan on the Sc correlation plot indicates a significant range in D_{Sc} (Fig. 6a). The scatter of Sc partitioning data in high-T samples indicates a lack of

equilibration at high temperature due to garnet resorption. Ti exhibits an irregular distribution between coexisting garnet and biotite (Fig. 6b). The concentrations of Ti are well above the detection limits (>20 times) in both minerals. Furthermore, there is no systematic difference in the distribution of Ti with metamorphic grade, even if only Ti-saturated (ilmenite-bearing) samples are considered. The V distribution pattern between garnet
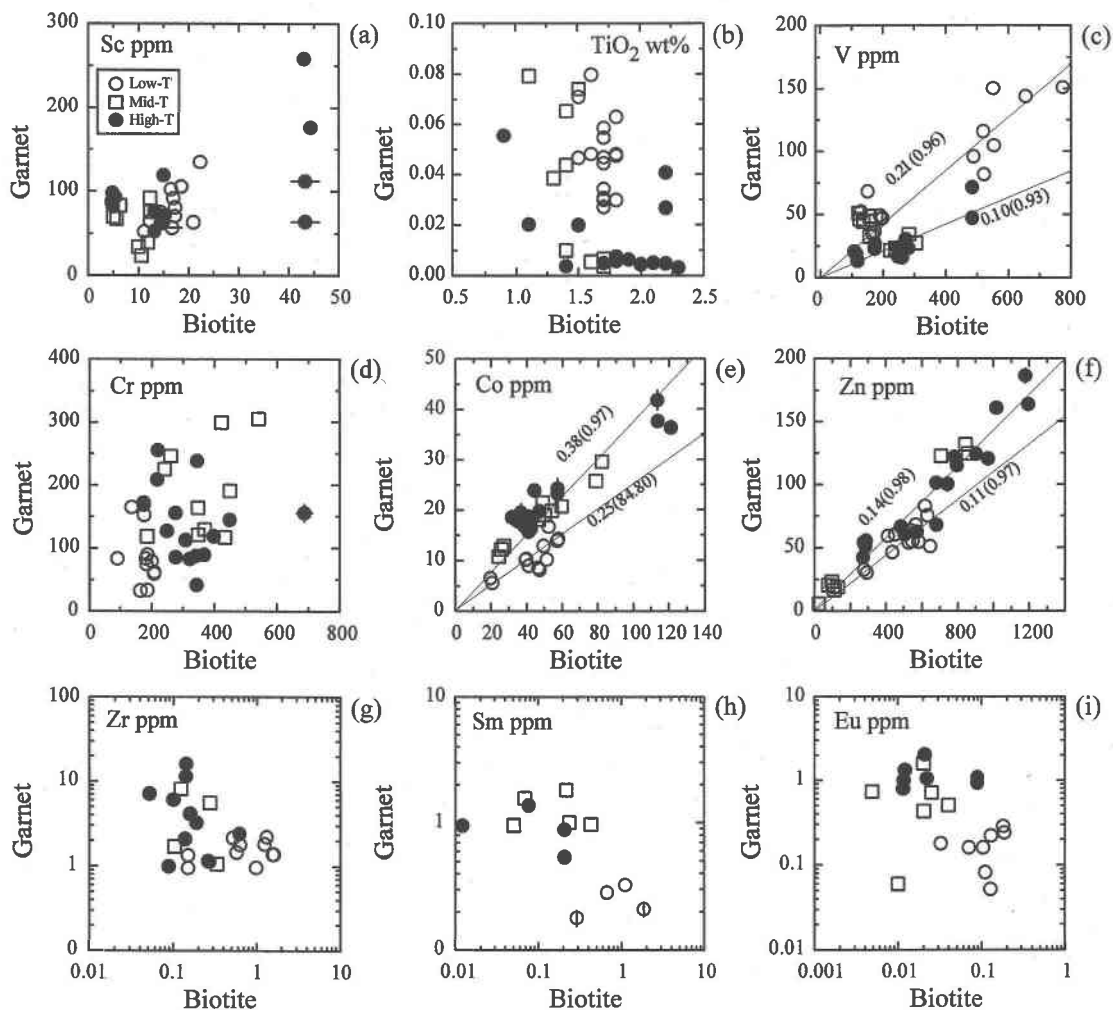
FIG. 6. Distribution diagrams illustrating the partitioning of Sc, Ti, V, Cr, Co, Zn, Zr, Sm and Eu between coexisting garnet and biotite. Diagonal lines represent least-square regression lines for low- and high-T samples. The values in parentheses represent r^2 of the regressions. Analytical error bars representing one standard deviation are smaller than the symbols, except where shown.

and biotite appears to be linear, with different patterns of distribution between low-temperature (slope = 0.21) and high-temperature (slope = 0.10) samples (Fig. 6c). The Cr correlation plot shows a broad scatter around a 2:1 line (Fig. 6d). Co and Zn show good correlation between coexisting garnet and biotite, with different distribution-coefficients at different metamorphic grades (Figs. 6e, f). There is a distinct difference in distribution coefficients D_{Zr}, D_{Sm} and D_{Eu} between low- and high-T samples although their concentrations are close to detection limits in either garnet or biotite (Figs. 6g, h, i).

Mean Nernst distribution coefficients were calculated from low-, mid- and high-T samples for the trace elements (Table 8). The formulation of the distribution coefficient (D_i or D_i^*) does not affect the relative order of trace-element enrichment with metamorphic grade. The D_i values for Sc, V, Cr and Co and the relative order of enrichments among them are similar to those in the literature (Table 8). However, direct comparisons are problematic, as most of the published analytical data were determined by bulk-mineral methods, which cannot be free from contamination and chemical zoning. Hickmott & Spear (1992) reported partitioning data

TABLE 7. REPRESENTATIVE VALUES OF D_i^* BETWEEN COEXISTING GARNET AND BIOTITE AND ESTIMATED TEMPERATURE OF METAMORPHISM (FERRY & SPEAR 1978)

Spl.	87-81	87-83			87-86		87-283		87-279		88-49		88-48		88-45		88-85		88-74		88-80		88-57		88-58	
Grt	F23	G1	C11	C24	C1	C8	C3	D2	D6	D1	A4	A45	D1	D3	E1	E7	C4	D10	C5	D8	B9	B5	A13	A9	B5	C4
Bt	F8	G12	C23	C9	C34	C4	C5	D5	D3	D3	A5	A1	D2	D4	E2	E4	C5	D11	C6	D9	B4	B6	A12	A12	B3	C3
Sc	6.0	6.4	5.6		4.4	4.3	5.8	6.3	5.5				3.6	6.6	14.0	12.6	17.8	18.3	5.1	5.0	4.2	6.3	2.7	1.6	4.5	4.2
Ti	0.05	0.05	0.05		0.03	0.03	0.03	0.05	0.03		0.01	0.01	0.05	0.07	0.01	0.01					0.02		0.02	0.03		
V	0.40	0.43	0.72		0.33	0.38	0.25	0.43	0.35		0.15	0.20	0.53	0.59	0.12	0.15	0.13	0.18	0.11	0.10	0.13	0.14	0.23	0.15	0.26	0.30
Cr	1.38		0.29			0.73	0.48	0.77	0.63		0.60	0.45	0.92	1.14	0.56	0.75	0.59	0.82	0.50	0.41	0.19	1.10	1.79	0.36	1.52	1.56
Mn	18	19	29		32	36	34	51	17	17					70	65	80	69	68	64	31	54	28	15	18	14
Co	0.27	0.27	0.34		0.25	0.26	0.18	0.19	0.35		0.40	0.36	0.38	0.47	0.50	0.46	0.62	0.53	0.35	0.32	0.45	0.40	0.44	0.43	0.44	0.47
Ni													0.90													
Cu																										
Zn	0.11	0.12	0.14		0.10	0.14	0.13	0.11	0.08		0.27		0.16	0.26	0.17	0.18	0.15	0.15	0.13	0.12	0.16	0.19	0.10	0.16	0.14	0.16
Sr																					0.56	0.26			0.01	
Y	1082	257	235		394	2586	174	156	115				95		993	1797					2019	1977			836	845
Zr	3	1	4			6	2	4	14	10			106		5	26	24		95	41	177	125				18
Nb										17																
Ba																										
La																										
Ce				0.02													0.01				0.01					
Pr				0.02									0.01	0.02	0.01	1.23					5.81	0.03				
Nd													0.08	0.07							0.58	0.05	0.05	0.05		
Sm		0.65			0.12			0.02		0.31			24.78	8.97	2.40	4.47	18.98				82.37		4.48	2.74		
Eu		2	6		2	4		1		7	9		23	14	30	87	51	107			72		11	13		
Gd		12	13		4	4	2			7			38		46	107	407				3064					
Tb		40	57		47		37	16		42			64		217	331										
Dy		221	96		264		136	42		84			175		911	1075										
Ho		383	86		711		125	138		167					2938	2903										
Er		822	81				214	161		153											4027					
Tm		4988	69				200			98			74								3953					
Yb		709	180				359	216		112			188	181	576	306					452		40	173		
Lu			200		1411					73											137	296				
Hf										1.46						0.39					19.04	8.42				
Ta			0.01	0.01																						
T(°C)	464	478	442	463	419	444	481	481	493	493	441	434	519	501	570	593	576	580	571	592	668	671	602	636	660	634

Elements	Low-T	Mid-T	High-T	Amphibolite facies[a]	Granulite facies[§]
Zn	0.11 ± 0.02	0.21 ± 0.06	0.15 ± 0.03	$0.37 \pm 0.15^{\dagger}$	-
V	0.25 ± 0.08	0.22 ± 0.13	0.11 ± 0.04	0.19 ± 0.13	0.15 ± 0.11
Co	0.26 ± 0.06	0.42 ± 0.05	0.44 ± 0.08	0.39 ± 0.20	0.56 ± 0.14
Cr	0.53 ± 0.34	0.63 ± 0.20	0.56 ± 0.36	0.76 ± 0.30	0.45 ± 0.49
Sc	4.91 ± 0.99	7.16 ± 4.35	8.49 ± 6.66	4.02 ± 2.15	6.51 ± 5.32

[a] Data from DeVore (1955), Turekian & Phinney (1962), Albee (1965) and Hietanen (1969).
[§] Data from Kretz (1959) and Engel & Engel (1960). [†] Data determined with the proton
microprobe by Hickmott & Spear (1992). Sample standard deviations are calculated at the 1σ
level.

derived from proton-microprobe measurements of Zn
in coexisting garnet and biotite from staurolite-bearing
metapelitic rocks. Their Zn partition coefficient, 0.37 ± 0.15 (1σ; two anomalously high values of D_{Zn} were re-
moved), is same as the value calculated in this study
(0.21 ± 0.06), within the permitted error (Table 8).

A close approach to equilibrium between coexisting
minerals is suggested by the approximately linear dis-
tributions of V, Co and Zn (Figs. 6c, e, f) and by their
intersections with the origin. This regularity also indi-
cates that the distribution of these trace elements is con-
trolled by crystal-chemical parameters and temperature,
which are discussed below.

DISCUSSION

Thermodynamic background

Trace-element partitioning can be viewed in terms
of simple exchange-reactions, for which the thermody-
namic basis is well established (e.g., Kretz 1961). For
example, Co partitioning between garnet and biotite can
be expressed by the reaction:

$$KCo_3AlSi_3O_{10}(OH)_2 + (Mg,Fe)_3Al_2Si_3O_{12} =$$
$$K(Mg,Fe)_3AlSi_3O_{10}(OH)_2 + Co_3Al_2Si_3O_{12} \quad (3)$$
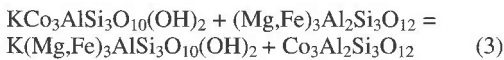
The distribution coefficient for reaction (3) is ap-
proximately equal to D_{Co}^*. If the two phases are ideal
crystalline solutions and follow Henry's law, at equilib-
rium

$$RT\ln D_i^* = -\Delta H_R + T\Delta S_R - (P-1)\Delta V_R \quad (4),$$

where R is the gas constant and T is the temperature in
Kelvins. ΔH_R, ΔS_R and ΔV_R are the enthalpy, entropy
and volume change of reaction, respectively. The effects
of pressure are predicted to be small owing to the small
change in volume for exchange reactions (McIntire
1963). This prediction is re-inforced by the results of
Guo & Green (1989, 1990), who found that the net ef-
fects of pressure are relatively small over pressure
ranges of 10–20 kbar for Ba partitioning between alkali
feldspar and melt. Thus in ideal solutions, the distribu-

tion coefficients will be controlled by temperature only.
If solid solution in garnet and biotite does not follow
Henry's law and assuming that ΔV_R can be neglected,
Eq. (4) is modified to:

$$RT\ln D_i^* = -\Delta H_R + T\Delta S_R + W \quad (5)$$

where the W term is composed of the product of the
interaction parameters at each site in each phase. At
constant temperature, the first two terms on the right-
hand side of Eq. (5) are constants, and $\ln D_i^*$ should be a
function of compositions only. Compositional effects on
trace-element partitioning are discussed in the follow-
ing section.

Compositional effects

A successful way of representing the compositional
dependencies of trace-element partition coefficients is
to compare the partitioning behavior of a trace element
with that of a major element. In examining such rela-
tionships, it is useful to consider atomic or molar pro-
portions and occupancies of cation sites, rather than
weight proportions (Beattie et al. 1991, Beattie 1993).
In addition, by considering the parameter $RT\ln D_i^*$ in-
stead of $\ln D_i^*$, we can simultaneously account for the
effects of temperature on the trace-element partitioning.

A negative correlation between Fe + Mg of garnet
versus Sc suggests that Sc substitutes into the X-sites of
garnet (Fig. 7a). Incorporation of Sc in the X sites is
considered to be charge-balanced by substitutions in-
volving Al and Si. Sm and Eu contents of garnet increase
with the X_{Mg} ratio of garnet (Fig. 7b), contradicting the
proposal of Caporuscio & Smyth (1990), that LREE
concentrations in garnet should increase with Ca con-
tents because of structural expansion of the 8-fold Y-
sites incurred by the increasing Ca content. The
substitution of REE into X-sites of garnet involves va-
cancies or coupled substitutions in order to maintain
charge balance. Jaffe (1951) suggested a mechanism
involving Y substitution for divalent cations in 8-fold
X-sites in garnet, with charge balance achieved by Al
substitution for Si in the 4-fold site, yielding a YAG-
type substitution. Enami et al. (1995) proposed a sub-
stitution involving Na, $Na(Y,Yb)Ca_{-2}$ at the X-sites. In
this study, Na was not detected by EMP in garnet, and
substitutions involving vacancies were not considered
because the analyzed grains commonly have total
REE+Y concentrations greater than 100 ppm and up to
220 ppm, amounts far in excess of those possible for
coupled vacancy defects (Beattie 1993). In biotite, there
is a broad negative correlation between Sc and Co con-
tents and ^{VI}Al (Fig. 7c). This indicates that Sc and Co
substitution involves a Tschermak-type substitution,
$SiMg^{IV}Al_{-1}{}^{VI}Al_{-1}$, where Sc and Co replace ^{VI}Al and
Mg, respectively. Concentrations of Sm, Eu and Gd in
biotite decrease with increasing X_{Mg} (Fig. 7d). REE in-
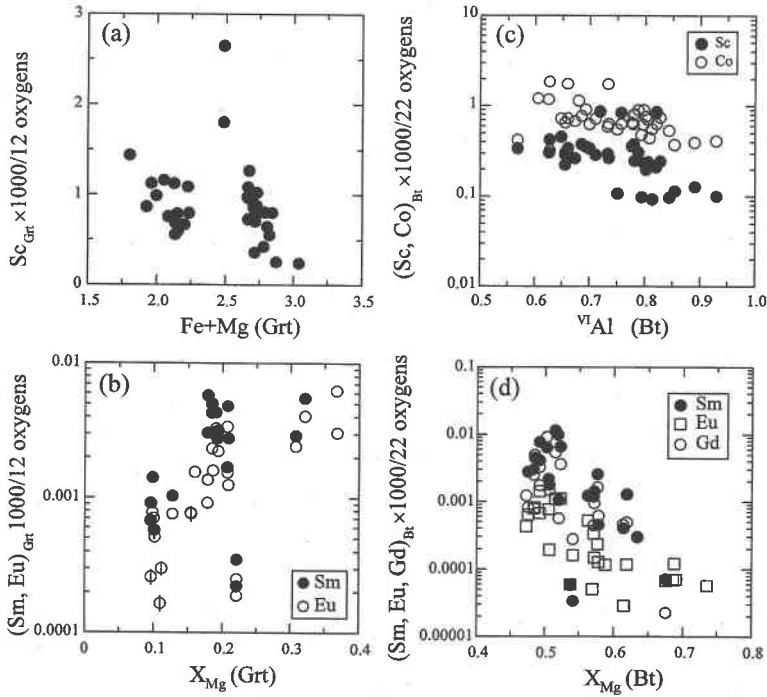corporation in the 12-fold coordinated sites in biotite

Fıg. 7.   Graphs showing trace-element concentrations *versus* major-element concentrations in garnet and biotite. Analytical error bars representing one standard deviation are smaller than the symbols, except where shown.

requires charge balance, but the mechanism cannot be determined with the data available. Fe^{2+} (0.92 Å) and Mg (0.89 Å) contents of garnet and biotite have no effect on Co (0.9 Å) and Zn (0.9 Å) concentrations in both of the minerals, reflecting the similarity of ionic radii among them and the operation of exchange reactions, $R^{2+}Mg_{-1}$, where R indicates divalent transition-element cations. No correlation was found between Fe^{3+} and trace elements in garnet, implying that all of the V may not occur as V^{3+}.

A plot of $RTlnD_{Sc}^{*}$ against ^{VI}Al of biotite (Fig. 8a) shows an overall positive correlation. This indicates that increasing octahedrally coordinated Al through a Tschermak substitution reduces the compatibility of Sc in biotite. Figure 8b shows a crystal-chemical coupling between Ti and Ca incorporation in garnet, as reported by Crawford (1974). Grossular has a larger unit-cell than almandine and pyrope (Novak & Gibbs 1971), which may facilitate Ti incorporation by expansion of the 6-fold Y-sites. There also is a bulk-composition effect, as shown by the different trend for samples 88–49 and 88–45. D_i values for Co and Zn show weak correlations with X_{Grs} (not shown). However, no correlations are found between Co and Zn with X_{Grs} in garnet in plots of $RTlnD_i^{*}$ *versus* X_{Grs}, indicating dependence of Co and

Zn partitioning on metamorphic temperature. D_{Zr}^{*} between garnet and biotite shows correlations with X_{Mg} of biotite and garnet (Fig. 8c), indicating that Zr substitutes in the 6-fold Y-sites of garnet. The partitioning of Sm, Eu and Gd seems to be controlled essentially by the X_{Mg} content of biotite (Fig. 8d) and garnet (not shown). Decreasing X_{Mg} values are accompanied by increasing X_K values in biotite, which leads to a secondary correlation of D_{Sm}^{*}, D_{Eu}^{*} and D_{Gd}^{*} with X_K (not shown); however, these correlations are not so marked as that with X_{Mg}. The strong correlations of D_{Sm}^{*} and D_{Gd}^{*} with X_{Mg} of both biotite and garnet across the entire compositional range indicate that the small crystal-chemical effects caused by the incorporation of Ca in garnet may have been masked by thermal effects. Among the trace elements studied here, Co and Zn show the least compositional effect on partitioning, implying ideal solid-solution or the same amount of non-ideality in both of the phases.

Thermal effects

The implications of the thermal dependence of trace-element partitioning between coexisting garnet and biotite are evident from Eq. (4). However, the effects of
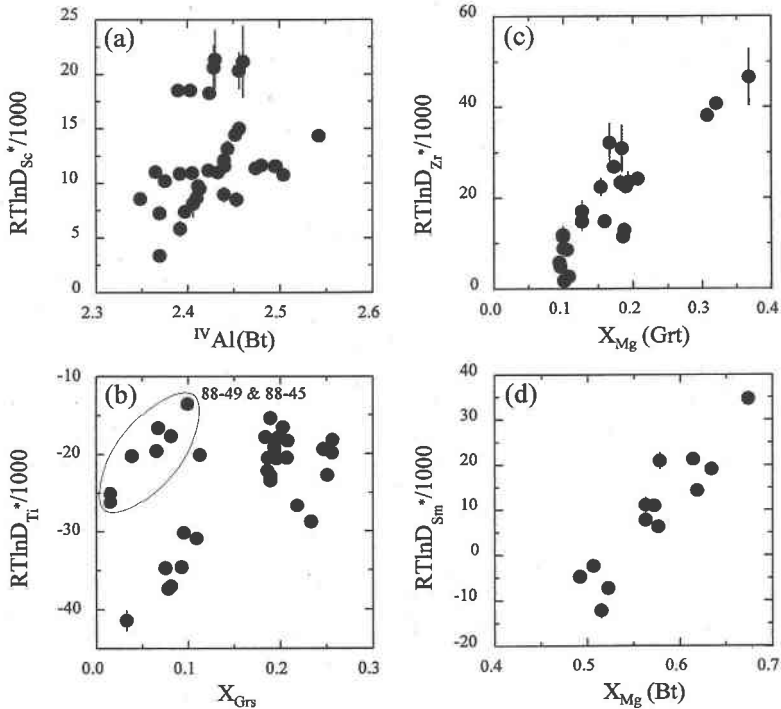
FIG. 8. $RT\ln D_i^*$ values of Sc, Ti, Zr and Sm plotted against various major-element parameters of garnet and biotite. Analytical error bars representing one standard deviation in the estimate of $RT\ln D_i^*/1000$ are smaller than the symbols, except where shown. The standard deviations of the estimates of D_i^* were calculated by propagating the error associated with counting statistics of each element in each phase; the relative standard deviations range from 1 to 15%, depending upon the element.

metamorphic temperature are difficult to predict for trace elements because enthalpy changes for exchange reactions are not available or cannot be calculated with sufficient precision using available calorimetric data. However, the thermal effects can be evaluated empirically if the temperature of equilibration can be determined for mineral pairs with known trace-element contents. In $\ln D_i^*$ *versus* $10^4/T$ diagrams, the slopes yield enthalpies that can be expressed as

$$\Delta H_r = \Delta H_m + \Delta H_f \qquad (6),$$

where ΔH_m is the heat of mixing, the change in enthalpy due to the change of chemical environment, and ΔH_f is heat of formation. These are the only possible contributions to ΔH_r, and in a system where solid solutions are ideal, the heat of reaction will simply equal the heat of fusion. For compatible elements, ΔH_m is possibly negative; for incompatible elements, ΔH_m is positive. In either case ΔH_f is negative, and ΔH_r will be positive if ΔH_f is less than ΔH_m.

This study does not reveal the thermal effects of Sc partitioning between coexisting garnet and biotite suggested by Engel & Engel (1960) and Krylova *et al.* (1970) from the epidote-amphibolite facies to the granulite facies. This may be due to loss of equilibrium compositions of Sc at the rims of garnet by resorption during retrograde metamorphism, together with the compositional effects from ^{VI}Al of biotite on the distribution of Sc. The chemical potential of Ti in garnet (or any other phase) is buffered by phase relations with minerals such as rutile, ilmenite and titanite. Thus, in a Ti-buffered system, the distribution of Ti may reflect changes in P and T at equilibrium (Ghent & Stout 1984, Hickmott & Spear 1992). The solubility of Ti in garnet is reported to increase with both P and T in Ti-buffered assemblages (Green & Sobolev 1975, Hickmott *et al.* 1987), contradicting the roughly decreasing Ti contents of garnet from low to high temperature (Fig. 4b). Thus, it can be concluded that crystal chemistry dominates the incorporation of Ti into garnet in the Labrador samples, as shown by coupling of Ti and Ca (Fig. 8b).

Values of $\ln D_V^*$ become progressively more negative with increasing temperature (Fig. 9a), a result that is not compatible with the general thermodynamic requirement that the D values for any element should tend towards 1 with increasing temperature. In contrast, the $\ln D_i^*$ values for Co and Zn tend toward 1 with increasing temperature (Fig. 9b). Values of $\ln D_{Co}^*$ increase continuously from -1.69 at about $450°C$ to -0.48 at about $700°C$, a factor of about 3. Values of $\ln D_{Zn}^*$ vary by a factor of 2 for the same range of temperature (Fig. 9c). Values of $\ln D_i^*$ for Zr, Sm, Eu and Gd show apparent positive correlations with metamorphic temperature and a systematic increase from Sm to Gd (Figs. 9d, e). This temperature dependence may be produced by the
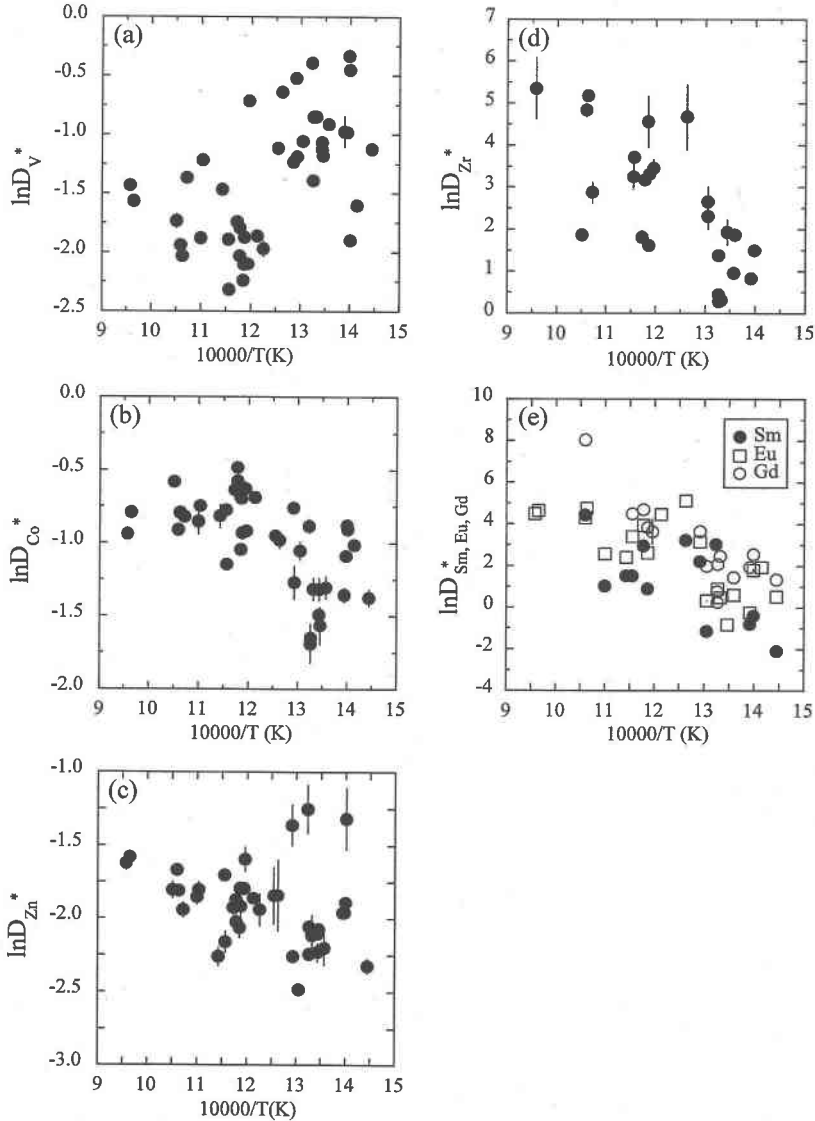
FIG. 9. Values of $\ln D_i^*$ for V, Co, Zn, Zr, Sm, Eu and Gd as a function of estimated temperatures of metamorphism. Analytical error bars representing one standard deviation in the estimate of $RT\ln D_i^*/1000$ are smaller than the symbols, except where shown. The standard deviations of the estimates of D_i^* were calculated by propagating the error associated with counting statistics of each element in each phase; the relative standard deviations range from 1 to 15%, depending upon the element.

greater thermal expansion of the garnet structure relative to that of the biotite (Smyth & Bish 1988), which would favor the incorporation of large cations at higher temperatures. Whereas this may be a purely thermal effect, it could also be due to the large analytical errors involved and the increasing Mg contents of both phases as temperature increases.

There is a positive correlation between $\ln D_V^*$ and $10^4/T$, whereas negative correlations exist for Co, Zn, Zr, Sm, Eu and Gd (Fig. 9). For the latter trace-elements, negative slopes on $\ln D_i^*$ *versus* $10^4/T$ diagrams imply that heats of reaction (ΔH_r) are positive, indicating that the partition of Co, Zn, Zr, Sm, Eu and Gd between garnet and biotite is dominantly controlled by the heats of mixing. This is simply another way of saying that the partitioning process is not ideal; were the heats of mixing small, the relations observed in Figure 9b–e would not be possible.

Structural effects

The main crystal-chemical constraints in trace-element partitioning are the charge and the ionic radius of the trace element, in relation to the nominal charge and volume of the host polyhedron (*e.g.*, Nagasawa 1966, Onuma *et al.* 1968, Brice 1975, Blundy & Wood 1994, Beattie 1994). Elastic and flexible crystal structures will most readily accommodate misfitting cations and therefore have the lowest interaction parameters.

Following the method of Blundy & Wood (1994), we have fitted our partitioning data for the X- and Y-sites, by weighted non-linear least-squares regression, to the relation:

$$D_i^* = D_o \exp\left[\frac{-4\pi E N_A}{RT}\left(\frac{r_o}{2}(r_i - r_o)^2 + \frac{1}{3}(r_i - r_o)^3\right)\right] \quad (7),$$

which relates the partition coefficients for some cation *i* of ionic radius r_i to the partition coefficient D_o for a cation whose radius equals the optimal site-radius, r_o. In this relation, E is the value of Young's modulus for the site, N_A is Avogadro's number, R is the gas constant and T is in Kelvins. By fitting the determined D_i^* values to Eq. (7), we can obtain best-fit values for D_o, E and r_o for each isovalent series. The results are listed in Table 9. For divalent cations, the calculated value of r_o for the X-sites, using the mean cation – oxygen distance for grossular (Smyth & Bish 1988) and the size of the O^{2-} ion (Shannon 1976), is consistent with the value of r_o regressed from the partitioning data (Table 9). As only three trivalent cations (Sm, Eu and Gd) are used in the regression of trivalent cations substituting into garnet X-sites, we have set r^{3+}_o equal to r^{2+}_o. For the same reason, we are forced to fix r_o for garnet Y-sites: our chosen value (0.54 Å) is the ionic radius of Al in grossular, which is a host cation on the Y-sites in grossular. The estimated Young's modulus for trivalent cations substi-

tuting on the X-site is larger than that of divalent cations, in keeping with the inferred higher elasticity when coupled substitutions are involved (Beattie 1994).

Divalent and trivalent cations except for Sc show good agreement with the regression curves, with maxima corresponding to the size of 6- and 8-fold-coordinated Y- and X-sites in garnet (Fig. 10). Thus, all these elements are incorporated into Y- and X-sites of garnet, and the partitioning of trivalent cations is charge-balanced by coupled substitutions. From ionic radius arguments alone, we anticipate that Sc^{3+} is incorporated into the X-sites of garnet. However, Sc plots above the parabola that describes partitioning of trivalent cations into the X-sites, and Sc does not gain any crystal-field stabilization energy (Schwarcz 1967). The mismatch between the regression line for the parabola for trivalent cations in X-sites and the distribution coefficient of Sc may be caused by the large errors involved in the determinations of distribution coefficients of the *REE*, and hence significant error in the location and size of the parabola for trivalent cations.

The slope of the parabolas is known to be a function of P and T (Bass 1995). For the data in this study, except for V, average trace-element partition coefficients for high-T samples are consistently higher than those of low-T samples (Fig. 6), supporting the controls of P and T on the trace-element partitioning between coexisting garnet and biotite. The different behavior of V distribution implies that V partitioning is largely controlled by crystal-chemical factors. However, it is debatable whether the results in this study can be explained entirely in terms of lattice elasticity, as the P and T ranges of the samples are relatively small (<250°C, <6 kbars). In addition, the high-T D_i^* values for divalent and trivalent cations for most samples, although greater than those for low-T samples (Fig. 6), do not allow definition of separate parabolas for high-temperature conditions. It is worth noting that elements away from the peaks of each parabola, such as Co, Zn, Sm and Nd,

TABLE 9. LATTICE SITE-PARAMETERS, AS OBTAINED BY REGRESSION OF GARNET/BIOTITE PARTITIONING DATA

Sites	Charge	E (kbar)	r_o (Å)	D_o
X	2+	7249 ± 101	1.02 ± 0.06	107 ± 2
			1.02#	
	3+	18029 ± 29	1.02ᶦ	23 ± 1
Y	3+	13644 ± 50	0.54#	7.8 ± 1.1
Bulk		1628*		

E is Young's modulus for the site. r_o is optimal site radius. D_o is partition coefficient for a cation with the optimum radius. # r_o is obtained by subtracting the ionic radius of the O^{2-} ion, 1.38 Å, (Shannon 1976) from the observed average cation-oxygen bond length (Smyth & Bish 1988). ᶦ r_o obtained from the regression for divalent cations in X-sites. * Measured Young's Modulus for the bulk crystals calculated at 740 K and 7 kbar (Bass 1995).
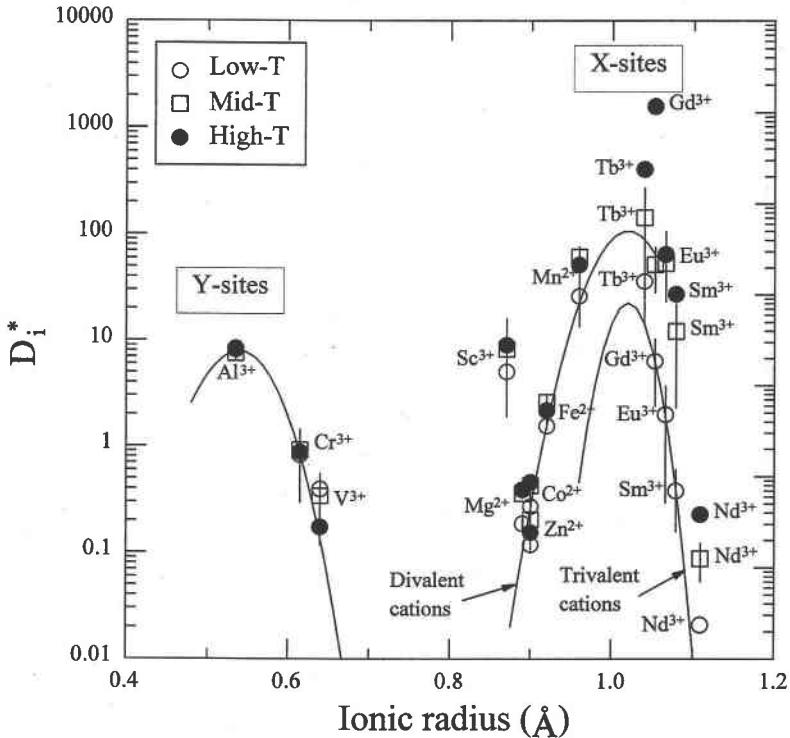
FIG. 10.   An Onuma diagram showing the estimated partition-coefficients plotted against ionic radius (Å) for the X and Y sites in garnet. The graph shows that the variation in trace-element partition coefficients is controlled by ionic radius and charge. The curves represent weighted non-linear regression fits for the garnet–biotite partitioning data. Standard deviations (1σ) are shown by vertical lines. The points for *REE* with no error bars represent single determinations.

exhibit greater change in distribution coefficients than elements in hinge areas, implying that elements whose ionic radius differs greatly from r_o experience more severe change in elasticity for a given change in P–T.

However, these elements are also subject to higher interaction energies owing to their larger misfit, resulting in stronger controls by crystal chemistry. The absence of compositional dependence of Co and Zn partitioning between coexisting garnet and biotite may be attributed to the similar degree of non-ideality in the two phases. The values of D_o, E and r_o regressed from garnet – biotite partitioning data can be used in conjunction with Eq. (6) to predict partition coefficients for trace elements that were not examined in this study.

CONCLUSIONS

Detailed trace-element analyses using LAM–ICP–MS, combined with results of major-element analyses of garnet and biotite from lower-greenschist to upper-

amphibolite-facies metamorphic rocks from western Labrador by electron microprobe, allow us to draw the following conclusions.

(1) Systematic distributions of some trace elements (*e.g.*, V, Cr, Co and Zn) between garnet and biotite are consistent with equilibrium partitioning during metamorphism.

(2) The trace-element proportions in garnet and biotite are mainly controlled by bulk composition and the assemblage of coexisting minerals. For instance, garnet and biotite in the staurolite zone are strongly depleted in Zn owing to the equilibration with staurolite. Such elemental signatures can contribute to deciphering reaction histories in favorable cases.

(3) Garnet and biotite studied here show correlations between trace and major elements, which support the existence of a major-element control on incorporation of some trace elements. For other trace elements, temperature may be an important factor in partitioning. For example, the partitioning of Sc between garnet and

biotite in the samples shows a dependence on ^{VI}Al content of biotite, but no dependence on temperature. The distribution of Ti is primarily controlled by the Ca content of garnet. On the other hand, D_V^*, D_{Zr}^*, D_{Sm}^*, D_{Eu}^* and D_{Gd}^* are controlled by both crystal-chemical factors and temperature. The partitioning of Co and Zn shows a temperature effect, with the least compositional effects; both elements partition preferentially into garnet at higher temperature.

(4) The partition coefficients between garnet and biotite exhibit dependence on ionic radius and charge. This suggests that trace-element partitioning occurs by substitution onto specific crystallographic sites in crystalline phases and that the partitioning of trivalent cations in X sites is charge-balanced by coupled substitutions.

None of the elements promises a simply applicable alternative "trace-element geothermometer" for greenschist- and amphibolite-facies metamorphic rocks. The scatter in plots of $\ln D_i^*$ versus $10^4/T$ is large, and in the case of V, Zr, Sm, Eu and Gd, the composition effects cannot be separated from thermal effects. However, these data do provide a series of tests for equilibrium between phases in metapelitic samples, and hence can be used to improve the choice of appropriate samples for other studies. Compositional ranges of trace elements and partition coefficients between coexisting garnet and biotite provide useful information for qualitative and quantitative modeling of reaction histories of metamorphic assemblages. The relationships between distribution coefficients and ionic radius can be used to predict partition coefficients of trace elements that have not been studied in this paper and also to choose trace elements for a possible future "trace-element geothermometer". The systematic trace-element distributions demonstrate that irregular partitioning of trace elements between garnet and biotite, suggested by several previous studies utilizing whole-mineral digestion techniques, may have been due at least in part to impurities and trace-element zoning, which are avoided with the in situ measurements by LAM–ICP–MS.

REFERENCES

ALBEE, A.L. (1965): Phase equilibria in three assemblages of kyanite-zone pelitic schists, Lincoln Mountain quadrangle, central Vermont. J. Petrol. 6, 246-301.

AYRES, M. & VANCE, D. (1994): Constraints on the thermal evolution of the Indian Himalaya from manganese and erbium distributions in metapelitic garnets. Mineral. Mag. 58A, 34-35 (abstr.).

BASS, J.D. (1995): Elasticity of minerals, glasses and melts. In Handbook of Physical Constants (T.J. Ahrens, ed.). Am. Geophys. Union, Ref., Shelf 2, 45-63.

BEATTIE, P. (1993): On the occurrence of apparent non-Henry's law behaviour in experimental partitioning studies. Geochim. Cosmochim. Acta 57, 47-55.

_____ (1994): Systematics and energetics of trace-element partitioning between olivine and silicate melts: implications for the nature of mineral/melt partitioning. Chem. Geol. 117, 57-71.

_____, FORD, C. & RUSSELL, D. (1991): Partition coefficients for olivine–melt and orthopyroxene–melt systems. Contrib. Mineral. Petrol. 109, 212-224.

BLUNDY, J. & WOOD, B. (1994): Prediction of crystal–melt partition coefficients from elastic moduli. Nature 372, 452-454.

BRICE, J.C. (1975): Some thermodynamic aspects of the growth of strained crystals. J. Crystal Growth 28, 249-253.

BROWN, D., RIVERS, T. & CALON, T. (1992): A structural analysis of a metamorphic fold–thrust belt, northeast Gagnon terrane, Grenville Province. Can. J. Earth Sci. 29, 1915-1927.

CAPORUSCIO, F.A. & SMYTH, J.R. (1990): Trace-element crystal chemistry of mantle eclogites. Contrib. Mineral. Petrol. 105, 550-561.

CONNELLY, J.N., VAN GOOL, J., RIVERS, T. & JAMES, D.T. (1996): Field guide to the geology of the Grenville province of western Labrador. In Proterozoic Evolution in the North Atlantic Realm, COPENA–ECSOOT–IBTA Conf., Field Excursion Guide 1.

CRAWFORD, M.L. (1974): Calcium zoning in almandine: a model based on plagioclase equilibria. In The Feldspars (W.S. McKenzie & J. Zussman, eds.). Manchester University Press, New York, N.Y. (629-644).

DAHL, P.S., WEHN D.C. & FELDMANN, S.G. (1993): The systematics of trace-element partitioning between coexisting muscovite and biotite in metamorphic rocks from the Black Hills, South Dakota, USA. Geochim. Cosmochim. Acta 57, 2487-2505.

DEVORE, G.W. (1955): The role of adsorption in the fractionation and distribution of elements. J. Geol. 63, 159-190.

ENAMI, M., CONG, B., YOSHIDA, T. & KAWABE, I. (1995): A mechanism for Na incorporation in garnet: an example from garnet in orthogneiss form the Su–Lu terrane, eastern China. *Am. Mineral.* **80**, 475-482.

ENGEL, A.E.J. & ENGEL, C.G. (1960): Progressive metamorphism and granitization of major paragneiss, northwest Adirondack Mountains, New York. II. Mineralogy. *Geol. Soc. Am., Bull.* **71**, 1-58.

FERRY, J.M. & SPEAR, F.S. (1978): Experimental calibration of the partitioning of Fe and Mg between biotite and garnet. *Contrib. Mineral. Petrol.* **66**, 113-117.

FRYER, B.J., JACKSON, S.E. & LONGERICH, H.P. (1995): The design, operation and role of the laser- ablation microprobe coupled with an inductively coupled plasma – mass spectrometer (LAM–ICP–MS) in the earth sciences. *Can. Mineral.* **33**, 303-312.

GHENT, E.D. & STOUT, M.Z. (1984): TiO_2 activity in metamorphosed pelitic and basic rocks: principles and applications to metamorphism in southeastern Canadian Cordillera. *Contrib. Mineral. Petrol.* **86**, 248-255.

GOVINDARAJU, K. (1994): 1994 compilation of working values and sample description for 383 geostandards. *Geostandards Newsletter* **18**.

GREEN, D.H. & SOBOLEV, N.V. (1975): Coexisting garnets and ilmenites synthesized at high pressure from pyrolite and olivine basanite and their significance for kimberlitic assemblages. *Contrib. Mineral. Petrol.* **50**, 217-229.

GUO, JINGFENG & GREEN, T.H. (1989): Barium partitioning between alkali feldspar and silicate melts at high temperature and pressure. *Contrib. Mineral. Petrol.* **102**, 328-335.

_____ & _____ (1990): Experimental study of barium partitioning between phlogopite and silicate liquid at upper-mantle pressure and temperature. *Lithos* **24**, 83-95.

HICKMOTT, D.D. & SHIMIZU, N. (1990): Trace-element zoning in garnet from the Kwoiek area, British Columbia: disequilibrium partitioning during garnet growth? *Contrib. Mineral. Petrol.* **104**, 619-630.

_____, _____, SPEAR, F.S. & SELVERSTONE, J. (1987): Trace-element zoning in a metamorphic garnet. *Geology* **15**, 573-576.

_____ & SPEAR, F.S. (1992): Major- and trace-element zoning in garnets from calcareous pelites in the NW Shelburne Falls quadrangle, Massachusetts: garnet growth histories in retrograded rocks. *J. Petrol.* **33**, 965-1005.

HIETANEN, A. (1969): Distribution of Fe and Mg between garnet, staurolite, and biotite in aluminum-rich schist in various metamorphic zones north of the Idaho batholith. *Am. J. Sci.* **267**, 422-456.

JACKSON, S.E., LONGERICH, H.P., DUNNING, G.R. & FRYER, B.J. (1992): The application of laser- ablation microprobe – inductively coupled plasma – mass spectrometry (LAM–

ICP–MS) to in situ trace-element determinations in minerals. *Can. Mineral.* **30**, 1049-1064.

JAFFE, H.W. (1951): The role of yttrium and other minor elements in the garnet group. *Am. Mineral.* **36**, 133-155.

JENNER, G.A., FOLEY, S.F., JACKSON, S.E., GREEN, T.H., FRYER, B.J. & LONGERICH, H.P. (1993): Determination of partition coefficients for trace-elements in high pressure–temperature experimental run products by laser ablation microprobe – inductively coupled plasma – mass spectrometry (LAM–ICP–MS). *Geochim. Cosmochim. Acta* **57**, 5099-5103.

KRETZ, R. (1959): Chemical study of garnet, biotite, and hornblende from gneisses of southwestern Québec, with emphasis on distribution of elements coexisting minerals. *J. Geol.* **67**, 371-402.

_____ (1961): Some applications of thermodynamics to coexisting minerals of variable composition. examples: orthopyroxene–clinopyroxene and orthopyroxene–garnet. *J. Geol.* **69**, 361- 387.

_____ (1983): Symbols for rock-forming minerals. *Am. Mineral.* **68**, 277-279.

KRYLOVA, M.D., DAGELAYSKIY, V.B. & ORLOVSKAYA, K.V. (1970): Distribution trends of scandium between the minerals of metamorphic rocks. *Geochem. Int.* **7**, 804-813.

LANZIROTTI, A. (1995): Yttrium zoning in metamorphic garnets. *Geochim. Cosmochim. Acta* **59**, 4105-4110.

LONGERICH, H.P. (1995): Analysis of pressed pellets of geological samples using wavelength-dispersive X-ray fluorescence spectrometry. *X-Ray Spectrom.* **24**, 123-136.

_____, GÜNTHER, D. & JACKSON, S.E. (1996a): Elemental fractionation in laser-ablation inductively-coupled mass-spectrometry. *Fresenius J. Anal. Chem.* **355**, 538-542.

_____, JACKSON, S.E. & GÜNTHER, D. (1996b): Laser ablation – inductively coupled plasma – mass spectrometric transient signal data acquisition and analyte concentration calculation. *J. Anal. Atomic Spec.* **11**, 899-904.

_____, JENNER, G.A., FRYER, B.J. & JACKSON, S.E. (1990): Inductively coupled plasma – mass spectrometric analysis of geological samples: a critical evaluation based on case studies. *Chem. Geol.* **83**, 105-118.

McINTIRE, W.L. (1963): Trace element partition coefficients – a review of theory and applications to geology. *Geochim. Cosmochim. Acta* **27**, 1209-1264.

MEAGHER, E.P. (1982): Silicate garnets. *In* Orthosilicates (P.H. Ribbe, ed.). *Rev. Mineral.* **5**, 25-67.

NAGASAWA, H. (1966): Trace element partition coefficient in ionic crystals. *Science* **152**, 767-769.

NIELSEN, R.H. (1985): A method for the elimination of the compositional dependence of trace element distribution coefficients. *Geochim. Cosmochim. Acta* **49**, 1775-1779.

_____ (1988): A model for the simulation of the combined major and trace element liquid lines of descent. *Geochim. Cosmochim. Acta* **52**, 27-38.

NOVAK, G.A. & GIBBS, G.V. (1971): The crystal chemistry of the silicate garnets. *Am. Mineral.* **56**, 791-825.

ONUMA, N., HIGUCHI, H., WAKITA, H. & NAGASAWA, H. (1968): Trace element partition between two pyroxenes and the host lava. *Earth Planet. Sci. Lett.* **5**, 47-51.

PEARCE, N.J.G., PERKINS, W.T., WESTGATE, J.A., GORDON, M.P., JACKSON, S.E., NEAL, C.R. & CHENERY, S.P. (1997): A compilation of new and published major and trace-element data for NIST SRM-610 and NIST SRM-612 glass reference materials. *Geostandards Newsletter* **21**, 115-144.

RIVERS, T. (1983): Progressive metamorphism of pelitic and quartzofeldsparthic rocks in the Grenville Province of western Labrador – tectonic implications of bathozone 6 assemblages. *Can. J. Earth Sci.* **20**, 1791-1804.

_____, VAN GOOL, J.A.M. & CONNELLY, J.N. (1993): Contrasting tectonic styles in the northern Grenville province: implications for the dynamics of orogenic fronts. *Geology* **21**, 1127-1130.

SCHWANDT, C.S., PAPIKE, J.J. & SHEARER, C.K. (1996): Trace-element zoning in pelitic garnet of the Black Hills, South Dakota. *Am. Mineral.* **81**, 1195-1207.

_____, _____, _____ & BREARLEY, A.J. (1993): A SIMS investigation of REE chemistry of garnet in garnetite associated with the Broken Hill Pb–Zn–Ag orebodies, Australia. *Can. Mineral.* **31**, 371-379.

SCHWARCZ, H.P. (1967): The effect of crystal field stabilization on the distribution of transition metals between metamorphic minerals. *Geochim. Cosmochim. Acta* **31**, 503-517.

SHANNON, R.D. (1976): Revised effective ionic radii and systematic studies of interatomic distances in halides and chalcogenides. *Acta Crystallogr.* **A32**, 751-767.

SMYTH, J.R. & BISH, D.L. (1988): *Crystal Structures and Cation Sites of the Rock-Forming Minerals*. Allen and Unwin, Boston, Massachusetts.

TAYLOR, R.P., JACKSON, S.E., LONGERICH, H.P. & WEBSTER, J.D. (1997): In situ trace-element analysis of individual silicate melt inclusions by laser ablation microprobe – inductively coupled plasma – mass spectrometry (LAM–ICP–MS). *Geochim. Cosmochim. Acta* **61**, 2559-2567.

TAYLOR, S.R. & MCLENNAN, S.M. (1985): *The Continental Crust: its Composition and Evolution*. Blackwell Scientific, Boston, Massachusetts.

TUREKIAN, K.K. & PHINNEY, W.C. (1962): The distribution of Ni, Co, Cr, Cu, Ba, and Sr between biotite garnet pairs in a metamorphic sequence. *Am. Mineral.* **47**, 1434-1441.

VAN GOOL, J.A.M. (1992): *The Grenville Front Foreland Fold-and-Thrust Belt in Southwestern Labrador: Mid-crustal Structural and Metamorphic Configuration of a Proterozoic Orogenic Thrust Wedge*. Ph.D. thesis, Memorial Univ. of Newfoundland, St. John's, Newfoundland.